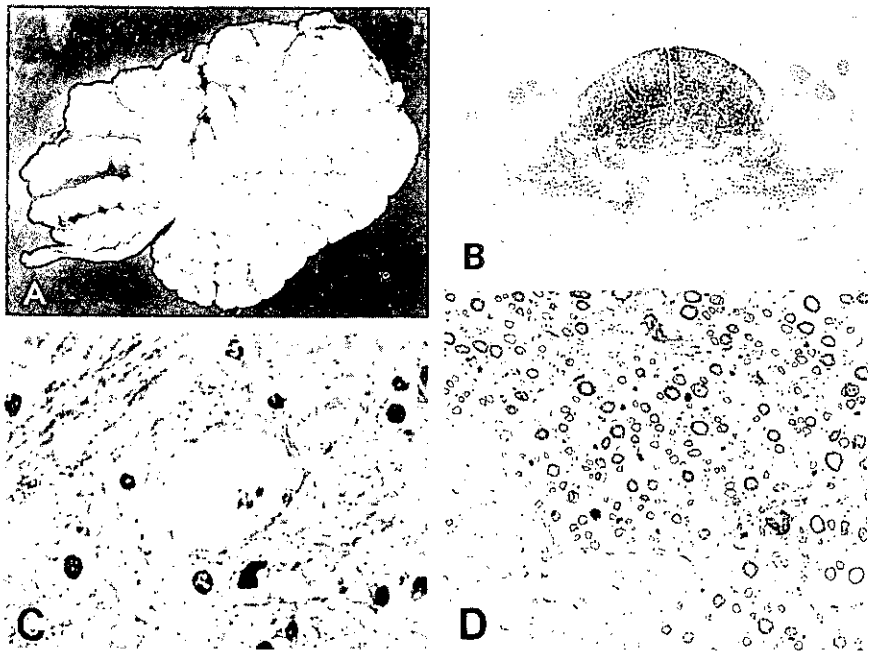

Figure (**A**) Mid-sagittal section of the cerebellar vermis showing predominant atrophy of the upper half portion. (**B**) Transverse section of the thoracic spinal cord (T8) showing atrophy of the central gray matter and degeneration of both corticospinal and spinocerebellar tracts. Kluver-Barerra stain. (**C**) A neuron containing Bunina bodies in the lumber anterior horn. H. E. x 540 (**D**) Lumbar anterior root showing a marked loss of myelinated fibers and endoneurial fibrosis. Toluidine blue stained Epon semithin section. x 220

SCA6 [7–9], despite the fact that the clinical course of this patient was relatively short because of concomitant affliction with ALS. In contrast to those reported by Yang, et al. [10], no findings suggestive of developmental anomaly such as ectopic Purkinje cells or aberrant sprouting of Purkinje dendrites could be found in this case.

The significant loss of Clarke neurons and secondary degeneration of the spinocerebellar tracts seen in the present case seems worthy of brief comment. Although usually clinically undetectable, the occurrence of Clarke nuclei degeneration has been well established in ALS in patients on prolonged ventilatory support [11], which may explain the degeneration of the cerebellar afferent in the present case. The cause of sudden death in our patient was unclear. However, Shimizu, et al. have reported that circulatory collapse and sudden death can develop in respiratory-dependent ALS patients in which sympathetic hyperactivity may play a causative role [12].

In conclusion, autopsy of a patient who clinically presented with SCA6 and motor neuron loss revealed the co-existence of typical histological features of ALS and those previously reported for SCA6. Immunohistochemisty for the α1A channel protein revealed characteristic cytoplasmic aggregates in the Purkinje cells but not in motor neurons of the spinal cord. These findings support the view that the present case is the result of a chance association between two relatively rare neurodegenerative diseases, although the possibility of motor involvement in SCA6 could not be completely excluded.

The authors thank Ms R Mimura, Department of Clinical Laboratory, National Chushin-Matsumoto Hospital, for her technical assistance.

References

1. Ohara S, Tsuyuzaki J, Hayashi R, Iwahashi T, Nakajima T, Maruyama T, Tokuda T, Nonaka I (2000) Motor neuron loss in a patient with spinocerebellar ataxia type 6: chance occurrence or causally related? J Neurol 247: 386–388
2. Leigh PN, Whitwell H, Harofalo O, Buller J, Swash M, MartinJE, Gallo J-M, Weller RO, Anderton BH (1991) Ubiquitin-immunoreactive intraneuronal inclusions in amyotrophic lateral sclerosis. Morphology, distribution, and specificity. Brain 114: 775–788
3. Suenaga T, Matsushima H, Nakamura S, Akiguchi I, Kimura J (1993) Ubiquitin-immunoreactive inclusions in anterior horn cells and hypoglossal neurons in a case with Joseph's disease. Acta Neuropathol (Berl) 85: 341–344
4. Schols L, Amoiridis G, Epplen A, Langkafel M, Przuntek H, Riess O (1996) Relations between genotype and phenotype in German patients with the Machado-Joseph disease mutation. J Neurol Neurosurg Psychiatry 61: 466–470
5. Klockgether T, Schols L, Abele M, Burk K, Topka H, Andres F, Amoiridis G, Ludtke R, Riess O, Laccone F, Dichgans J (1999) Age related axonal neuropathy in apinocerebellar ataxia3/Machado-Joseph disease(SCA3/MJD). J Neurol Neurosurg Psychiatry 66: 222–224
6. Gomez CM, Thompson RM, Gammack JT, Perlman SL, Dobyns WB, Truwit CL, Zee DS, Clark HB, Anderson JH (1997) Spinocerebellar ataxia type 6: Gaze-evoked and vertical nystagmus, Purkinje cell degeneration, and variable age of onset. Ann Neurol 42: 933–950
7. Takahashi H, Ikeuchi T, Honma Y, Hayashi S, Tuji S (1998) Autosomal dominant cerebellar ataxia (SCA6): clinical, genetic and neuropathological study in a family. Acta Neuropathol (Berl) 95: 333–337
8. Ishikawa K, Watanabe M, Yoshizawa K, Fujita T, Iwamoto H, Yoshizawa K, Harada K, Nakamagoe K, Komatsuzaki Y, Satoh A, Doi M, Ogata T, Kanazawa I, Shoji S, Mizusawa H (1999) Clinical, neuropathological, and molecular study in two families with spinocerebellar ataxia type 6 (SCA6). J Neurol Neurosurg Psychiatry 67: 86–89
9. Sasaki H, Kojima H, Yabe I, Tashiro K, Hamada T, Sawa H, Hiraga H, Nagashima K (1998) Neuropathological and molecular studies of spinocerebellar ataxia type 6 (SCA6). Acta Neuropathol (Berl) 95: 199–204
10. Yang Q, Hashizume Y, Yoshida M, Wang Y, Goto Y, Mitsuma N, Ishikawa K, Mizusawa H (2000) Morphological Purkinje cell changes in spinocerebellar ataxia type 6. Acta Neuropathol (Berl) 100: 371–376

11. Takahashi H, Oyanagi K, Ohama E, Ikuta F (1992) Clarke's column in sporadic amyotrophic lateral sclerosis. Acta Neuropathol (Berl) 84: 465–470
12. Shimizu T, Hayashi H, Kato S, Hayashi M, Tanabe H, Oda M (1994) Circulatory collapse and sudden death in respirator-dependent amyotrophic lateral sclerosis. J Neurol Sci 124: 45–55

S. Ohara, MD (✉) · T. Iwahashi, MD · T. Oide, MD
Department of Neurology
National Chushin-Matsumoto Hospital
811, Kotobuki
Matsumoto 399-0021, Japan
Fax: +81-263/86-3190

R. Hayashi, MD
Department of Medicine (Neurology)
Shinshu University School of Medicine
3-1-1 Asahi
Matsumoto 390–8621, Japan

T. Nakajima, MD
Department of Neurology
National Saigata Hospital
468-1 Saigata
Ogata-machi, nakakubiki-gun
Niigata 949-3173, Japan

K. Ishikawa, MD · H. Mizusawa, MD
Department of Neurology
Tokyo Medical Dental College
1-5-45 Yushima, Bunkyo-ku
Tokyo 113-8596, Japan

THE JOURNAL OF BIOLOGICAL CHEMISTRY
Vol. 277, No. 21, Issue of May 24, pp. 19213–19219, 2002
Printed in U.S.A.

Biochemical Characterization of the Core Structure of α-Synuclein Filaments*

Received for publication, November 2, 2001, and in revised form, March 11, 2002
Published, JBC Papers in Press, March 13, 2002, DOI 10.1074/jbc.M110551200

Hirotomo Miake‡§, Hidehiro Mizusawa§, Takeshi Iwatsubo‡¶, and Masato Hasegawa‡‖¶**

From the ‡Department of Neuropathology and Neuroscience, Graduate School of Pharmaceutical Sciences, University of Tokyo, 7-3-1 Hongo, Bunkyo-ku, Tokyo 113-0033, the §Department of Neurology and Neurological Science, Graduate School of Medicine, Tokyo Medical and Dental University, 1-5-45 Yushima, Bunkyo-ku, Tokyo 113-8519, and the ‖Department of Molecular Neurobiology, Tokyo Institute of Psychiatry, Tokyo Metropolitan Organization for Medical Research, 2-1-8 Kamikitazawa, Setagaya-ku, Tokyo 156-8585, Japan

Intracellular filamentous aggregates comprised of α-synuclein such as Lewy bodies and glial cytoplasmic inclusions are the defining hallmarks of a subset of neurodegenerative diseases including Parkinson's disease, dementia with Lewy bodies, and multiple system atrophy. We have analyzed biochemical and structural properties of α-synuclein filaments assembled *in vitro* or extracted from brains of patients with multiple system atrophy and found that both types of filaments are insoluble to detergents and partially resistant to proteinase K digestion. Immunoelectron microscopy and immunoblot analysis showed that both amino and carboxyl termini of α-synuclein in *in vitro* assembled filaments were degraded by proteinase K treatment, whereas the central portion of α-synuclein is resistant to proteinase K and retains filamentous structures. Protein sequencing and mass spectrometric analyses of the proteinase K-resistant, minimal fragment of 7 kDa revealed that amino acid residues 31–109 of α-synuclein constitute the core unit of the filaments. These observations suggest that the central half of the α-synuclein polypeptide, containing five tandem repeats as well as a part of the carboxyl-terminal acidic region, forms the core structure of α-synuclein filaments, which is coated by the amino- and carboxyl-terminal portions at the periphery.

Filamentous cytoplasmic inclusion bodies comprised of α-synuclein in neurons or glial cells are the hallmark lesions of a group of neurodegenerative diseases collectively referred to as synucleinopathies (1). In Parkinson's disease (PD)[1] and dementia with Lewy bodies (DLB), α-synuclein is deposited as Lewy bodies and Lewy neurites that accumulate in cell bodies or neuronal processes (2–4), whereas filamentous α-synuclein aggregates are predominantly found in oligodendrocytes as glial cytoplasmic inclusions (GCIs) in multiple system atrophy (MSA) (5–7). The following evidence strongly implicates the deposition of α-synuclein in the pathogenesis of these neurodegenerative disorders. 1) Two missense mutations (A53T and A30P) in the α-synuclein gene that cosegregate with the onset of PD have been identified in kindreds of autosomal dominantly inherited familial PD (8, 9). 2) Immunohistochemical and biochemical analysis of PD, DLB, and MSA brains have revealed widespread deposition of α-synuclein in the brains of patients with either sporadic or familial forms of PD, as well as in DLB and MSA (10, 11), in which α-synuclein has been shown to form the major filamentous component of inclusion bodies (6, 10, 12). 3) Recombinant α-synuclein proteins assemble into filaments *in vitro* that closely resemble those found in LB and GCIs, whereas other members of synuclein family proteins, *i.e.* β-synuclein and γ-synuclein, neither deposit in brains nor assemble into filaments (13–15). 4) Missense mutations (A53T and A30P) identified in familial PD have been shown to increase the propensity of α-synuclein to form filaments or oligomers (16–20).

α-Synuclein is a 140-amino acid, heat-stable protein, harboring seven imperfect tandem repeat sequences in the amino-terminal half (Fig. 1*A*), followed by a hydrophobic central region (referred to as the NAC portion) and an acidic carboxyl terminus. α-Synuclein is abundantly expressed in neurons as a cytosolic protein that is localized to presynaptic termini, although it has been shown that a proportion of α-synuclein is associated with membranes (21, 22). Circular dichroism spectra analysis of recombinant proteins revealed that α-synuclein is a natively unfolded protein with little ordered secondary structure (23). Further structural analyses have shown that full-length or carboxyl-terminal-truncated recombinant α-synuclein can assemble into straight filaments 5–10 nm wide that closely resemble filaments isolated from PD, DLB, or MSA brains (13–15). X-ray fiber diffraction and electron diffraction analyses have shown that a transition from random coil to a cross-β-sheet structure underlies the assembly of α-synuclein into filaments (15). Recent studies have shown that residues 71–82 of α-synuclein, which are absent in β-synuclein, play a crucial role in its assembly into filaments (24). However, γ-synuclein also harbors a hydrophobic stretch similar to that of α-synuclein (and especially a homologous portion to residues 71–82 of α-synuclein) although γ-synuclein poorly assembles into filaments (14, 15).

To learn more about the mechanisms underlying the assembly of the natively unfolded α-synuclein protein into β-sheet-rich filaments, we studied the biochemical properties of α-synuclein filaments, especially their structural stability to protease digestion. Here we have shown that α-synuclein filaments assembled *in vitro* or recovered from MSA brains that

* This work was supported by grants-in-aid from the Ministry of Education, Science, and Culture (to M. H. and T. I.). The costs of publication of this article were defrayed in part by the payment of page charges. This article must therefore be hereby marked "*advertisement*" in accordance with 18 U.S.C. Section 1734 solely to indicate this fact.

¶ Both contributors served as senior authors.

** To whom correspondence should be addressed: Dept. of Molecular Neurobiology, Tokyo Inst. of Psychiatry, Tokyo Metropolitan Organization for Medical Research, 2-1-8 Kamikitazawa, Setagaya-ku, Tokyo 156-8585, Japan. Tel.: 81-3-3304-5701; Fax: 81-3-3329-8035; E-mail: masato@prit.go.jp.

[1] The abbreviations used are: PD, Parkinson's disease; DLB, dementia with Lewy bodies; GCIs, glial cytoplasmic inclusions; MSA, multiple system atrophy; Tricine, *N*-[2-hydroxy-1,1-bis(hydroxymethyl)ethyl] glycine; HPLC, high pressure liquid chromatography; MALDI-TOF, matrix-assisted laser desorption/ionization-time of flight.

are morphologically similar to each other share the following biochemical characteristics: (i) insolubility in detergents (Triton X or Sarkosyl) but high solubility in urea or SDS, and (ii) resistance of a subdomain of α-synuclein against proteinase K treatment. We propose that the proteinase K-resistant 7-kDa fragment comprised of residues 31–109 of α-synuclein may represent the core unit of α-synuclein filaments, which contributes to the structural stability of these filaments.

EXPERIMENTAL PROCEDURES

Antibodies—Monoclonal antibody LB509 was raised against isolated Lewy bodies, and the epitope was localized to residues 121/122 of α-synuclein (25). Syn102 was raised against recombinant α-synuclein with an epitope within residues 131–140 (7, 26). No. 36 is an antiserum against a synthetic peptide corresponding to residues 1–10 of α-synuclein. NAC1 raised against a synthetic peptide corresponding to residues 75–91 of α-synuclein is a gift from Dr. Jäkälä (27).

Extraction of Dispersed α-Synuclein Filaments from MSA Brains—α-Synuclein filaments derived from glial cytoplasmic inclusions were extracted from frozen cerebella from patients with MSA or from normal individuals as controls. 0.5–1 g of brain tissue was homogenized in 10 volumes of buffer A (50 mM Tris-HCl, pH 7.5, 1 mM EGTA, 1 mM dithiothreitol) and centrifuged at 1,000 × *g* for 10 min. The supernatants were ultracentrifuged at 350,000 × *g* for 20 min, and the resulting pellets were sequentially extracted by homogenization followed by ultracentrifugation in buffer A containing 1% Triton X-100 and then in 10% sucrose and 0.5 M NaCl. The pellets were homogenized in buffer A containing 1% Sarkosyl, 10% sucrose, and 0.5 M NaCl and incubated at 37 °C for 1 h. After centrifugation at 27,000 × *g* for 20 min, the supernatants were further centrifuged at 350,000 × *g* for 20 min. The resulting pellets were suspended in a 0.5-fold volume of 50 mM Tris-HCl buffer (pH 7.5) and subjected to proteinase K treatment and immunoelectron microscopic analysis of α-synuclein filaments. This Sarkosyl-insoluble fraction was further homogenized in buffer A containing 8 M urea, and the urea-soluble fraction was obtained by ultracentrifugation. Each supernatant fraction was denatured in SDS sample buffer, separated by 15% Tris/Tricine gels, and analyzed by immunoblotting as described (11).

In Vitro Assembly and Ultrastructural and Biochemical Analyses of Recombinant α-Synuclein into Filaments—Recombinant α-synuclein was expressed in *Escherichia coli* BL21 and purified by boiling treatment and then Q-Sepharose ion exchange chromatography followed by separation by reverse phase-HPLC on an Aquapore RP300 column as described (28). For assembly, recombinant α-synuclein was prepared at a concentration of 4 mg/ml in 50 μl of 30 mM Tris-HCl (pH 7.5) and incubated at 37 °C with shaking at 250 rpm in an incubator. After incubation for 48 h, aliquots (0.5–1 μl) were placed on 400-mesh carbon-coated grids and negatively stained with 2% lithium phosphotungstate and observed by JEOL-1200EX. Immunoelectron microscopic analysis was performed as described (10). Briefly, after blocking with 10% calf serum, the grids were incubated with primary antibodies (Syn102, NAC1, or no. 36) diluted at appropriate concentrations for 2 h, followed by incubation with secondary antibodies conjugated with 5-nm gold particles (Sigma). The grids were stained with 2% lithium phosphotungstate prior to observation by electron microscopy. For differential solubilization of α-synuclein filaments, aliquots of assembly mixtures were dispersed by sonication in 10 volumes of buffer A and then centrifuged at 350,000 × *g* for 20 min. The resulting pellets were extracted with 10 volumes of buffer A containing 1% Triton X-100. After centrifugation, the Triton-insoluble pellets were homogenized in 1% Sarkosyl using sonication. The Sarkosyl-insoluble pellets were further extracted in 8 M urea. Each supernatant fraction was dissolved in SDS sample buffer and analyzed by SDS-PAGE.

Proteinase K Treatment of α-Synuclein Filaments—Sarkosyl-insoluble α-synuclein filaments extracted from brains of patients with MSA or Tris-soluble α-synuclein from control brains were treated with 1, 100, 500, or 1,000 μg/ml proteinase K at 37 °C for 30–60 min. The protein concentration of each fraction was adjusted to 2 mg/ml. *In vitro* assembled α-synuclein filaments and unassembled recombinant α-synuclein were treated with proteinase K at various concentrations of 2–1,000 μg/ml at 37 °C for 30–60 min. The reaction was stopped by boiling for 5 min. After centrifugation, the resulting pellets were dissolved in 8 M urea containing 2% SDS and analyzed by immunoblotting with LB509, Syn102, NAC1, or no. 36. Proteinase K-treated filaments were also analyzed by immunoelectron microscopy.

Protein Chemical Analysis of Proteinase K-resistant Core of α-Synuclein—*In vitro* assembled α-synuclein filaments and unassembled α-synuclein in soluble form were treated with 10 μg/ml proteinase K for 30 min. The digests were dissolved in SDS sample buffer, separated by SDS-PAGE, transferred to polyvinylidene difluoride membranes, and visualized by staining with Coomassie Brilliant Blue. The amino-terminal sequences of the major three bands migrating at 7, 8, and 9 kDa were directly analyzed by a protein sequencer (ABI492 protein sequencer) as described (29). Analysis of the proteinase K-resistant 7-kDa fragment was performed by treating the assembled and unassembled α-synuclein with 500 μg/ml proteinase K for 60 min, followed by boiling for 5 min, and solubilization in 6 M guanidine HCl. The digests were separated on an Aquapore RP300 column (2.1 × 30 mm, Applied Biosystems) by HPLC (Hewlett-Packard, Model 1100) with a linear gradient of 0–48% acetonitrile in 0.1% trifluoroacetic acid for 16 min at a flow rate of 0.2 ml/min. Aliquots of the fractions were lyophilized, subjected to SDS-PAGE, and analyzed by immunoblotting with NAC1. Mass spectral analysis was performed by a Voyager-DE Pro MALDI-TOF mass spectrometer (PerSeptive Biosystems).

RESULTS

Previous studies have shown that recombinant α-synuclein forms filaments that closely resemble those isolated from brains of patients with PD, DLB, and MSA *in vitro*. To verify the morphological and biochemical characteristics of synthetic α-synuclein filaments, we have compared their ultrastructure and solubility with those isolated from brains of patients with MSA (Fig. 1*B*). Incubation of purified recombinant α-synuclein at 37 °C for 48 h with continuous shaking resulted in the formation of abundant filaments (Fig. 1*C*). These filaments were 50–700 nm long and 5–10 nm wide, as previously documented (15). These filaments appeared as straight filaments that were very similar to those extracted from MSA brains.

To biochemically characterize the α-synuclein filaments, we performed differential extraction of α-synuclein from brain tissues and *in vitro* assembled filaments. Frozen tissues from control and MSA brains were sequentially extracted with Tris-HCl buffer, 1% Triton X-100, 1% Sarkosyl, and 8 M urea. Extracted proteins were separated by SDS-PAGE and analyzed by immunoblotting with LB509. A 15-kDa polypeptide strongly immunoreactive for LB509 was detected in Tris-soluble and Triton-soluble fractions from both control and MSA brains. The amounts of α-synuclein in these fractions were slightly smaller in MSA brains compared with control brains. In contrast, LB509 immunoreactive polypeptides migrating at similar positions to normal α-synuclein were detected in the Sarkosyl-insoluble, urea-soluble fraction of MSA brain (Fig. 1*D*), whereas no α-synuclein immunoreactivities were observed in the same fractions of control brains. Immunoelectron microscopic observation of the Sarkosyl-insoluble fraction from MSA brains showed filaments that were labeled by multiple anti-α-synuclein antibodies. The extraction patterns of α-synuclein aggregates in MSA brains were similar to that observed by Dickson *et al.* (11) as well as to those in other synucleinopathies including DLB (30) and Hallervorden-Spatz disease,[2] suggesting that filamentous α-synuclein aggregates deposited in synucleinopathy brains exhibit similar insolubility profiles (*i.e.* Sarkosyl-insoluble and urea-soluble). The amounts of Sarkosyl-insoluble α-synuclein appeared to correlate with the density of GCIs as judged by semiquantitative evaluation of the amount of α-synuclein-positive aggregates by immunostaining of the smears of the brain homogenates (data not shown).

Similarly, *in vitro* assembled α-synuclein filaments were sequentially extracted by Tris-HCl, 1% Triton X-100, 1% Sarkosyl, and 8 M urea, together with unassembled α-synuclein incubated without shaking and analyzed by immunoblotting. As shown in Fig. 1*E*, unassembled α-synuclein was totally recov-

[2] H. Miake, H. Mizusawa, T. Iwatsubo, and M. Hasegawa, unpublished observations.

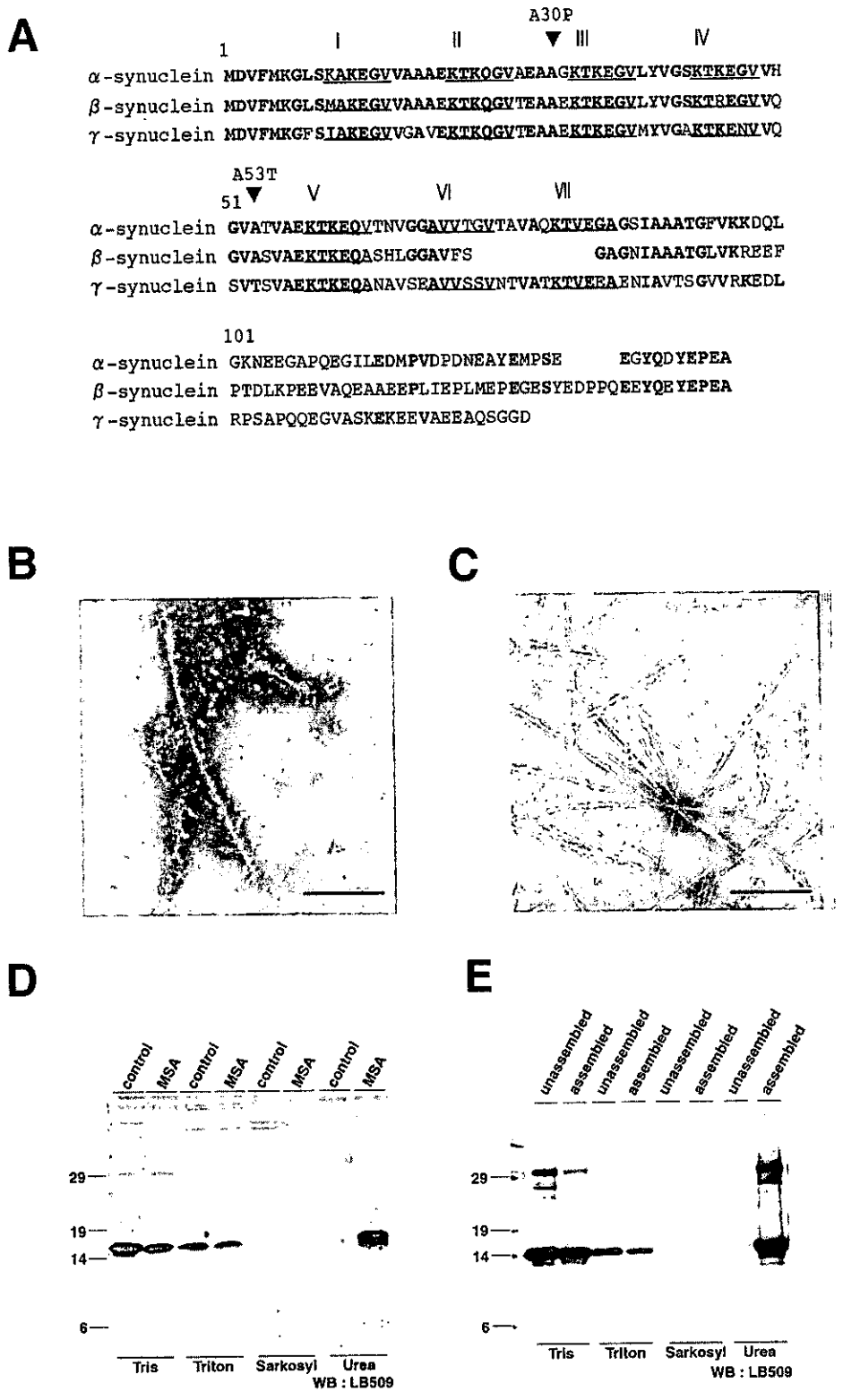

FIG. 1. **Ultrastructural and biochemical characteristics of α-synuclein filaments derived from MSA brains and assembled *in vitro* from recombinant proteins.** *A*, sequence alignment of human α-, β-, and γ-synuclein. The *underlined sequences* indicate five to seven tandem repeat sequences found in each synuclein. Amino acid residues of β- or γ-synucleins identical to those in α-synuclein are in *bold letters*. *A30P* and *A53T* mutations linked to familial PD also are shown. *B* and *C*, immunoelectron microscopic observation of dispersed filaments extracted from MSA brains (*B*, LB509/10 nm immunogold) and negatively stained electron micrograms from assembled recombinant α-synuclein protein *in vitro* (*C*). *Scale bar* represents 100 nm. *D* and *E*, differential solubilization profiles of α-synuclein from control and MSA brains (*D*), as well as from *in vitro* assembled filaments (*assembled*) and controls (*unassembled*) (*E*) revealed by immunoblotting with LB509. Buffers used for extraction are shown *below* the *lanes*. Molecular mass standards are shown in kilodaltons.

ered in Tris-HCl and Triton X-soluble fractions, without any immunoreactive substances detected in Sarkosyl-insoluble fractions. In sharp contrast, a ~15-kDa protein as well as additional polypeptides migrating at ~25–30 kDa in a Sarkosyl-insoluble, urea-soluble fraction of *in vitro* assembled α-synuclein showed strong immunoreactivity for LB509, the latter presumably representing α-synuclein dimers. Electron microscopic observation of the Sarkosyl-insoluble fraction of *in vitro* assembled α-synuclein confirmed the preservation of filamentous structures after extraction with 1% Triton X and 1% Sarkosyl. Taken together, synthetic α-synuclein filaments share a number of biochemical as well as morphological characteristics (*i.e.* solubility profiles, molecular size, and ultrastructure) with those recovered from inclusion bodies in synucleinopathy brains.

We next examined the structural stability of α-synuclein filaments by treating them with proteinase K. Tris-soluble fractions from control brains containing abundant normal α-synuclein and Sarkosyl-insoluble fractions from MSA brains rich in insoluble α-synuclein filaments were treated with 1

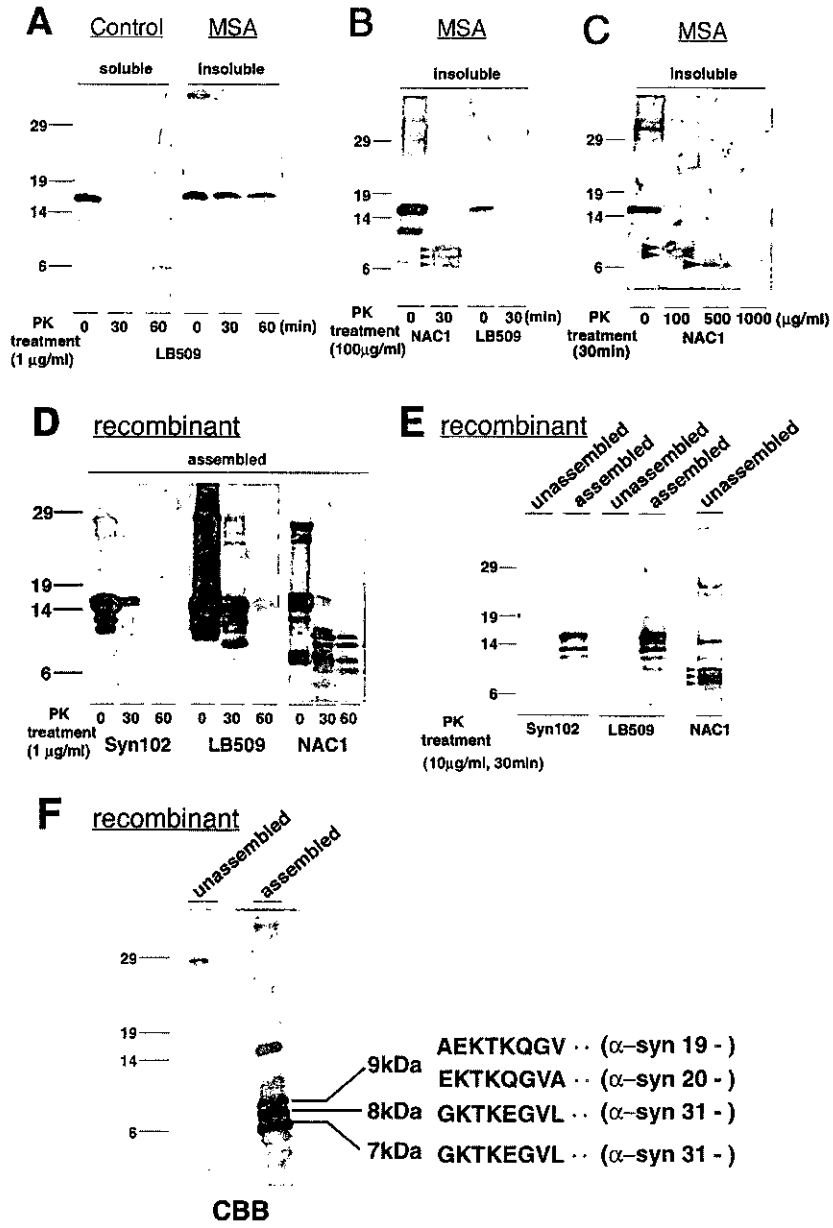

FIG. 2. **Proteinase K treatment of Sarkosyl-insoluble α-synuclein from MSA brains and *in vitro* assembled filaments from recombinant α-synuclein.** *A*, Tris-soluble fractions from control human brain (*left panel*) and Sarkosyl-insoluble fractions from MSA brain (*right panel*) were treated with 1 μg/ml proteinase K for 0, 30, and 60 min and analyzed by immunoblotting with LB509. *B*, Sarkosyl-insoluble fractions from MSA brain prior to (*0 min*) and after treatment with 100 μg/ml proteinase K for 30 min were analyzed by immunoblotting with NAC1 (*left panel*) and LB509 (*right panel*). *C*, Sarkosyl-insoluble fractions from MSA brain prior to (*0 min*) and after treatment with 100, 500, and 1,000 μg/ml proteinase K for 30 min were analyzed by immunoblotting with NAC1. *D*, *in vitro* assembled filaments from recombinant α-synuclein were treated with 1 μg/ml proteinase K for 0, 30, and 60 min and analyzed by immunoblotting with Syn102, LB509, and NAC1. *E*, *in vitro* assembled filaments from recombinant α-synuclein and unassembled controls were treated with 10 μg/ml proteinase K for 30 min and analyzed by immunoblotting with Syn102, LB509, and NAC1. Note that ~7–9-kDa bands were detected after proteinase K treatment by NAC1 both in Sarkosyl-insoluble fractions of MSA brain (*B*, *arrowheads*) and assembled α-synuclein (*E*, *arrowheads*), but Syn102 or LB509 failed to label these polypeptides. *F*, unassembled and assembled recombinant α-synuclein treated by proteinase K (10 μg/ml, 30 min) were separated by SDS-PAGE and stained with Coomassie Brilliant Blue. Amino acid sequences derived from polypeptides migrating at 9, 8, and 7 kDa, as well as the corresponding amino-terminal positions in human α-synuclein, are shown at the *right* of the *panel*.

μg/ml proteinase K, and digestion of α-synuclein was monitored by immunoblotting with LB509. Immunoreactivities for α-synuclein in Tris-soluble fractions disappeared after proteinase K treatment for 30 min. In contrast, the amount as well as banding patterns of α-synuclein in the Sarkosyl-insoluble fraction remained almost unchanged until 60 min of treatment (Fig. 2*A*). Soluble α-synuclein added to Sarkosyl-insoluble fractions from control brains was also readily degraded by proteinase K treatment (data not shown), indicating that the stability of Sarkosyl-insoluble α-synuclein to proteinase K is not due to interference by contaminants in this fraction. These results suggest that the filamentous form of α-synuclein in Sarkosyl-insoluble fractions is resistant to proteinase K digestion.

Sarkosyl-insoluble α-synuclein from MSA brains was further analyzed by immunoblotting with an additional anti-α-synuclein antibody NAC1, which recognizes the central hydrophobic region (*i.e.* NAC domain, residues 75–91) of α-synuclein, using higher concentrations of proteinase K (Fig. 2*B*). Prior to proteinase K treatment, NAC1 reacted with the major ~15-kDa polypeptide (migrating at the same position as full-length α-synuclein), as well as with additional minor bands migrating at ~6–12 kDa. After treatment with 100 μg/ml proteinase K, NAC1 exclusively reacted with ~7–9-kDa polypeptides (Fig. 2*B*, *arrowheads*), whereas α-synuclein immunoreactive bands migrating at higher molecular weight ranges (including full-length α-synuclein) were almost completely abolished. The ~7–9-kDa bands were not recognized by LB509, the epitope of which is located around residues 121/122 at the carboxyl terminus of α-synuclein. The 7-kDa band was still detected after the treatment with 500 μg/ml proteinase K with NAC1, although it disappeared by the 1,000 μg/ml proteinase K treatment (Fig. 2*C*), suggesting that these ~7–9-kDa polypeptides corresponded to the core portion of α-synuclein filaments that acquired high resistance to protease digestion. To further characterize the proteinase K-resistant α-synuclein fragments, *in vitro* assembled filaments were treated with 1 μg/ml proteinase K for 30–60 min and analyzed by immunoblotting with Syn102, LB509, and NAC1. Immunoreactivities of Syn102 or LB509 were almost completely abolished by the proteinase K treatment for 60 min, whereas ~7–11-kDa bands were detected in the assembled filament fraction with NAC1 (Fig. 2*D*). Similar results were obtained in the experiment with 10 μg/ml proteinase K treatment for 30 min. NAC1 detected ~7–9-kDa polypeptides in the assembled filament fraction (Fig. 2*E*, *ar-*

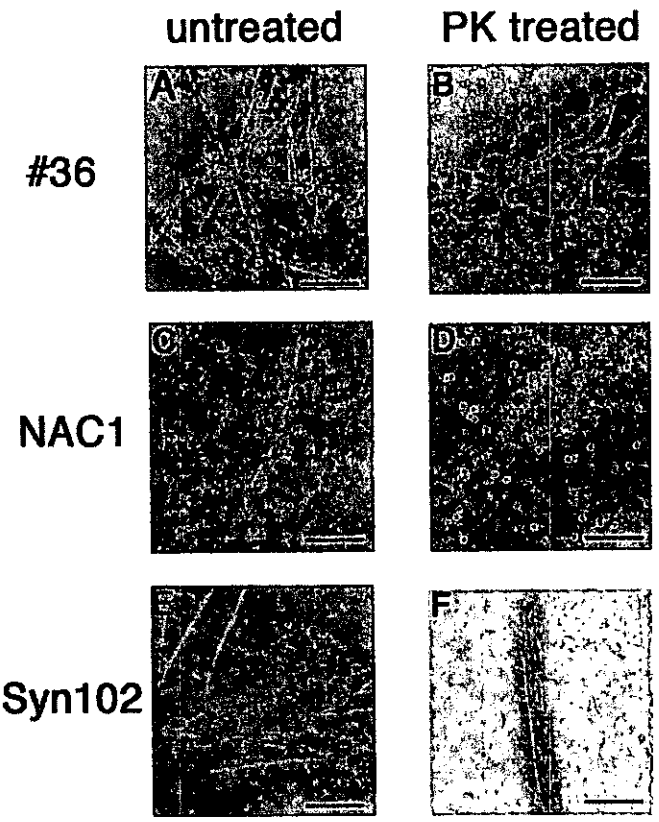

FIG. 3. **Immunoelectron microscopic analysis of assembled α-synuclein filaments with or without proteinase K treatment.** *In vitro* assembled filaments from recombinant α-synuclein prior to (*A*, *C*, *E*) or after proteinase K treatment (*B*, *D*, *F*) were immunolabeled by no. 36 (*A* and *B*), NAC1 (*C* and *D*), and Syn102 (*E* and *F*), followed by decoration with 5-nm gold particles and observed by negative staining. *Scale bar* represents 100 nm.

rowheads), exhibiting a similar pattern to those observed in the proteinase K-treated Sarkosyl-insoluble fractions of MSA brains (Fig. 2*B*, *arrowheads*), whereas antibodies to the carboxyl terminus of α-synuclein (*i.e.* LB509 and Syn102) only labeled the ~10–15-kDa bands. Unassembled α-synuclein digested by 10 μg/ml proteinase K did not yield any immunoreactive fragments, suggesting that α-synuclein was totally degraded in this condition (Fig. 2*E*).

To further analyze these proteinase K-resistant α-synuclein fragments by protein chemical methods, larger amounts (18 μg) of α-synuclein proteins in assembled or unassembled states were treated with proteinase K (10 μg/ml), separated by SDS-PAGE, transferred to polyvinylidene difluoride membranes, and stained with Coomassie Brilliant Blue. The amino-terminal sequences of the three major bands migrating at 7, 8, and 9 kDa detected in proteinase K-treated α-synuclein filaments were directly analyzed by a protein sequencer. Analysis of amino acid sequences of the 7- and 8-kDa bands revealed an identical amino-terminal sequence, GKTKEGVLYV, that corresponded to residues 31–40 of α-synuclein. The 9-kDa band gave two sequences, *i.e.* AEKTKQGVAE and EKTKQGVAEA, which corresponded to residues 19–28 and 20–29 of α-synuclein, respectively (Fig. 2*F*). Thus, both the 7- and 8-kDa proteinase K-resistant fragments consisted of polypeptides starting at the same amino terminus (*i.e.* residue 31 of α-synuclein) but ending at different carboxyl-terminal positions.

To investigate the relationship between the proteinase K-resistant ~7–9-kDa fragments and the integrity of α-synuclein filaments, we examined the ultrastructure as well as immunoreactivities of α-synuclein filaments prior to and after proteinase K treatment by immunoelectron microscopy (Fig. 3). Prior to proteinase K treatment, the filaments were positively labeled by antibodies against the amino- (Fig. 3*A*, *no. 36*) and carboxyl- (Fig. 3*E*, *Syn102*) terminal portions of α-synuclein, whereas NAC1 failed to label them (Fig. 3*C*). After proteinase K treatment, these filaments still retained their filamentous nature, but the mean diameters were decreased by ~20% (untreated, 12.3 ± 0.5 μm; proteinase K-treated, 9.8 ± 2.3 μm), and immunoreactivities for the amino (no. 36) and carboxyl (Syn102) termini were abolished. In sharp contrast, the filaments became immunoreactive for NAC1, which recognizes the mid-portion of α-synuclein. These results suggest that both the amino- and carboxyl-terminal regions of α-synuclein are structurally labile and cleaved off from the filaments by proteinase K digestion, whereas the central region containing the hydrophobic NAC portion represents the core structure of filaments that is resistant to protease treatment.

To unequivocally define the structure of the minimal fragment that constitutes the protease-resistant core of α-synuclein filaments, *in vitro* assembled α-synuclein filaments were treated with various concentrations of proteinase K ranging from 2 to 1,000 μg/ml. The NAC1 immunoreactive 7-kDa polypeptide remained undigested even by treatment with 1,000 μg/ml proteinase K, whereas other fragments including the 6-kDa species disappeared with increasing concentrations of proteinase K (Fig. 4*A*). This strongly suggested that the 7-kDa fragment corresponds to the highly stable, protease-resistant core unit of the α-synuclein filaments. To determine the exact structure of the proteinase K-resistant 7-kDa polypeptide, assembled α-synuclein filaments and unassembled α-synuclein proteins were treated with 500 μg/ml proteinase K, and the digests were dissolved in 6 M guanidine HCl and separated by reverse phase-HPLC. When the HPLC profiles of unassembled and filamentous α-synuclein were carefully compared after treatment with 500 μg/ml proteinase K, one peak was unique to assembled filament digests (Fig. 4*B*, *peak 9*); other peaks were derived from fragments of proteinase K, because identical peaks were observed by incubation without α-synuclein (data not shown). Immunoblotting of these HPLC fractions with NAC1 confirmed that the 7-kDa α-synuclein fragment was recovered in fraction 9 (Fig. 4, *B* and *C*). MALDI-TOF mass analysis of fraction 9 gave signals corresponding to a molecular mass of 7873.5, which nearly matched to that of residues 31–109 of human α-synuclein (predicted average mass: 7869) (Fig. 4*D*). These results strongly suggested that residues 31–109 of α-synuclein represent the proteinase K-resistant core unit of α-synuclein filaments.

DISCUSSION

The mechanisms by which α-synuclein is assembled into highly ordered filaments and forms intracellular inclusions in the brains of patients with synucleinopathies including PD, DLB, and MSA are unknown. It has been shown that recombinant α-synuclein can assemble into filaments that closely resemble the abnormal α-synuclein filaments in synucleinopathy brains (12). Thus, *in vitro* modeling of α-synuclein assembly is a useful strategy for the study of the molecular mechanisms of α-synuclein fibril formation as well as for screening of small molecules that affect the formation of pathological α-synuclein filaments.

In this study, we have shown that the *in vitro* assembled α-synuclein filaments closely resemble the pathological filaments of synucleinopathy brains in their biochemical and structural characteristics. *In vitro* assembled α-synuclein filaments and those from synucleinopathy brains shared very similar solubility profiles, *i.e.* insolubility in detergents (Triton X and Sarkosyl) and effective solubilization in high concentrations of urea. Furthermore, proteinase K treatment revealed

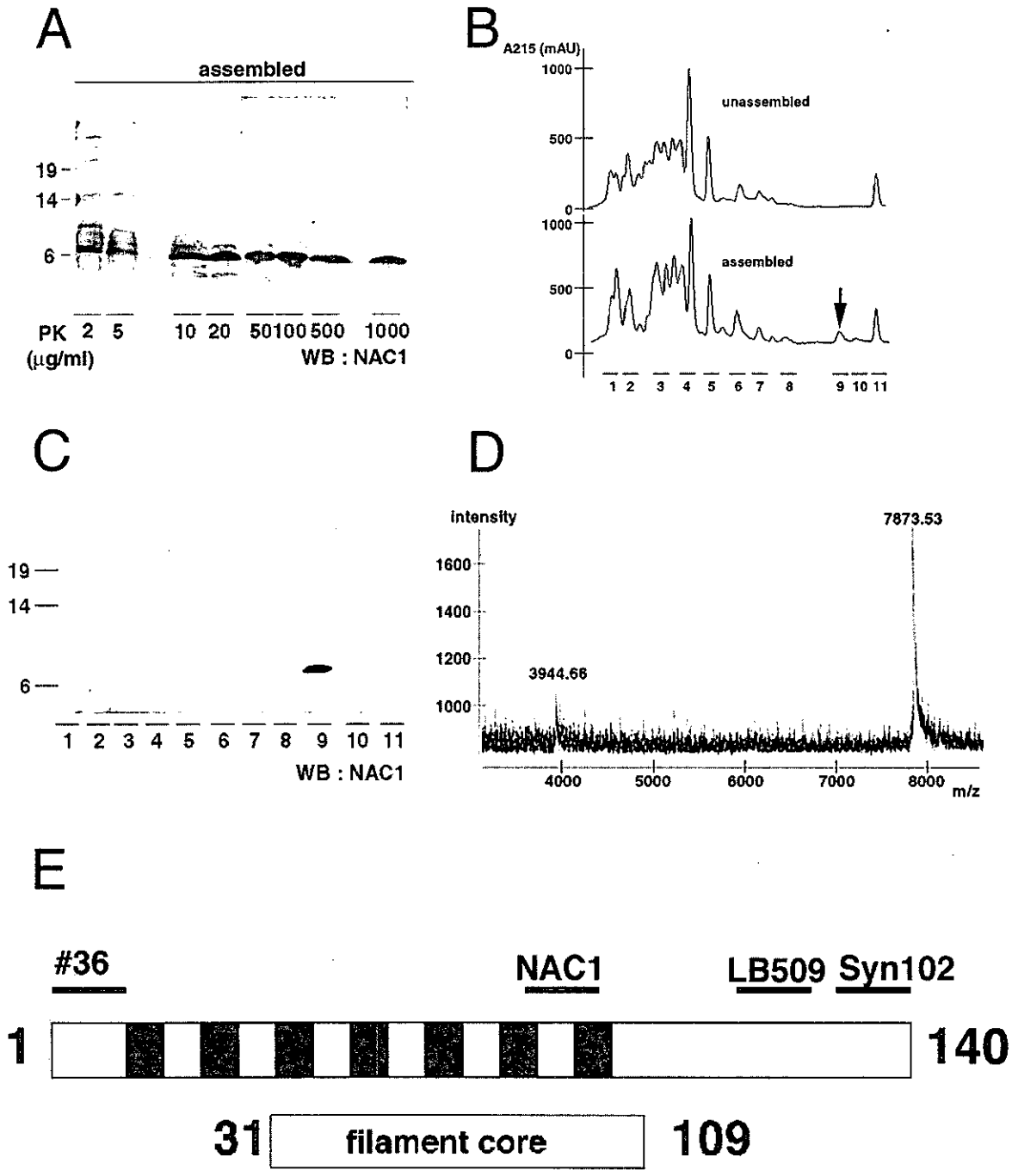

FIG. 4. **Purification and mass spectrometric analysis of the proteinase K-resistant 7-kDa fragment of α-synuclein filaments.** *A*, *in vitro* assembled α-synuclein filaments were treated with various concentrations of proteinase K (*PK μg/ml*, indicated *below* the *lanes*) and analyzed by immunoblotting with NAC1. *B*, separation profiles of *in vitro* assembled and unassembled α-synuclein proteins treated with proteinase K (500 μg/ml, 30 min) by reverse phase-HPLC on an Aquapore RP300 column. The *arrow* in the *lower panel* indicates a peak unique to assembled α-synuclein. *C*, immunoblot analysis of fractions separated in *B* with NAC1. *D*, MALDI-TOF mass spectrometry spectrogram of purified ~7-kDa proteinase K-resistant fragments of α-synuclein filaments. *E*, *schematic diagram* of the location of the ~7-kDa core of the α-synuclein filament.

that these two types of α-synuclein filaments show very similar resistance profiles to protease digestion.

Biochemical analysis of the proteinase K-resistant α-synuclein filament cores strongly suggested that the ~7–9-kDa fragments truncated at amino and carboxyl termini constitute the core portion of α-synuclein filaments. Giasson *et al.* (24) have reported similar proteinase K-resistant α-synuclein fragments, of which F1 and F2 fragments may correspond to our 8 and 7-kDa fragments, respectively. Conway *et al.* (20) have also reported a similar proteinase K-resistant α-synuclein fragment that may correspond to our 7-kDa fragment. We have further extended the characterization of the proteinase K-resistant α-synuclein core fragments by two complementary strategies, *i.e.* immunoelectron microscopy and protein chemical analysis.

Immunoelectron microscopic analysis showed that intact α-synuclein filaments are labeled by antibodies that recognize the amino or carboxyl termini of α-synuclein (no. 36 and Syn102, respectively), whereas an antibody that recognizes the central region of α-synuclein (NAC1) failed to label them. In sharp contrast, proteinase K treatment abolished the immunoreactivities for the amino- and carboxyl-terminal portions, whereas NAC1 immunoreactivity was retrieved, probably because removal of the surface structures exposed the antigen buried at the filament cores. Taken together with the immu-

nochemical data discussed above, it is strongly suggested that the central region of α-synuclein (encompassing the NAC1 epitope) constitutes the proteinase K-resistant core of α-synuclein filaments. Our observation that treatment of tissue sections with proteinase K or formic acid strongly enhanced the NAC1 immunoreactivities of synucleinopathy lesions on tissue sections (data not shown) may support this view.

Protein sequence and mass spectrometric analyses of the proteinase K-resistant fragments revealed that the central portion of α-synuclein corresponding to amino acid residues 31–109, which is half the size of holoprotein, constitutes the core of α-synuclein filaments. Recently, Giasson *et al.* (24) reported that the 12-amino acid stretch (^{71}VTGVTAVAQKTV^{82}) within the central hydrophobic region of α-synuclein is necessary and sufficient for its fibril formation, based on the sequence differences between α- and β-synucleins. However, the reason why γ-synuclein, which contains a hydrophobic stretch similar to that of α-synuclein (see Fig. 1*A*), poorly assembles into filaments (14, 15) is unknown. It is tempting to speculate that the carboxyl-terminal region of our 7-kDa fragment (residues 98–109), which is unique to α-synuclein but not found in β- or γ-synucleins, may contribute to its fibril formation. It is also interesting to note that the amino acid residues substituted by missense mutations linked to familial PD are located within (A53T) or adjacent to (A30P) this 7-kDa core fragment. The pathogenic effects of these mutations to promote formation of α-synuclein filaments or oligomers could be related to their effects on the conformational changes of this core portion. Further studies using variously modified or truncated recombinant α-synuclein are needed to clarify these points.

There are a number of interesting similarities between α-synuclein filaments deposited in synucleinopathy brains and tau filaments in Alzheimer's disease or tauopathy brains. Tau is a microtubule-associated protein harboring three or four tandem repeat sequences that serve as the microtubule binding domain. Tau can also be assembled into filaments *in vitro* from holoprotein or microtubule binding domain fragments (31–33). Using treatment by various proteases, it has also been shown that ~7–15-kDa fragments containing microtubule binding tandem repeats represent the protease-resistant core of the tau filaments that contributes to their stability (29, 34, 35). The amino- and carboxyl-terminal portions of tau are located peripheral to this core and constitute the superficial layer of filaments as a fuzzy coat (34, 35). It is tempting to speculate that there may be a common mechanism between α-synuclein and tau filaments whereby basic charged, tandem repeat sequences of 80~95 amino acids in size form detergent-insoluble, protease-resistant cores of highly ordered filaments from natively unfolded neuronal cytosolic proteins. Further structural analyses of pathological α-synuclein filaments will pave the way to unravel the mechanism whereby abnormal fibrous protein aggregates are formed and lead to neuronal dysfunction and eventually death in a wide variety of neurodegenerative disorders.

Acknowledgments—We thank Dr. Michel Goedert for a cDNA encoding human α-synuclein, Dr. Virginia M.-Y. Lee for Syn102, Dr. Pekka Jäkälä for NAC1, Dr. Yasuo Ihara for making MALDI-TOF mass available and Minami Baba, Akihiko Koyama, and Hideo Fujiwara for helpful discussions.

REFERENCES

1. Goedert, M. (2001) *Curr. Opin. Genet. Dev.* **11,** 343–351
2. Spillantini, M. G., Schmidt, M. L., Lee, V. M.-Y., Trojanowski, J. Q., Jakes, R., and Goedert, M. (1997) *Nature* **388,** 839–840
3. Baba, M., Nakajo, S., Tu, P.-H., Tomita, T., Nakaya, K., Lee, V. M.-Y., Trojanowski, J. Q., and Iwatsubo, T. (1998) *Am. J. Pathol.* **152,** 879–884
4. Irizarry, M. C., Growdon, W., Gomez-Isla, T., Newell, K., George, J. M., Clayton, D. F., and Hyman, B. T. (1998) *J. Neuropathol. Exp. Neurol.* **57,** 334–337
5. Wakabayashi, K., Yoshimoto, M., Tsuji, S., and Takahashi, H. (1998) *Neurosci. Lett.* **249,** 180–182
6. Spillantini, M. G., Crowther, R. A., Jakes, R., Cairns, N. J., Lantos, P. L., and Goedert, M. (1998) *Neurosci. Lett.* **251,** 205–208
7. Tu, P.-H., Galvin, J. E., Baba, M., Giasson, B., Tomita, T., Leight, S., Nakajo, S., Iwatsubo, T., Trojanowski, J. Q., and Lee V. M.-Y. (1998) *Ann. Neurol.* **44,** 415–422
8. Polymeropoulos, M. H., Lavedan, C., Leroy, E., Ide, S. E., Dehejia, A., Dutra, A., Pike, B., Root, H., Rubenstein, J., Boyer, R., Stenroos, E. S., Chandrasekharappa, S., Athanassiadou, A., Papapetropoulos, T., Johnson, W. G., Lazzarini, A. M., Duvoisin, R. C., Iorio, G. D., Golbe, L. I., and Nussbaum, R. L. (1997) *Science* **276,** 2045–2047
9. Krüger, R., Kuhn, W., Müller, T., Woitalla, D., Graeber, M., Kösel, S., Przuntek, H., Epplen, J. T., Schöls, L., and Riess. O. (1998) *Nat. Genet.* **18,** 106–108
10. Spillantini, M. G., Crowther, R. A., Jakes, R., Hasegawa, M., and Goedert, M. (1998) *Proc. Natl. Acad. Sci. U. S. A.* **95,** 6469–6473
11. Dickson, D. W., Liu, W.-K., Hardy, J., Farrer, M., Mehta, N., Uitti, R., Mark, M., Zimmerman T., Golbe, L., Sage, J., Sima, A., D'Amato, C., Albin, R., Gilman, S., and Yen, S.-H. (1999) *Am. J. Pathol.* **155,** 1241–1251
12. Crowther, R. A., Jakes, R., Spillantini, M. G., and Goedert, M. (1998) *FEBS Lett.* **436,** 309–312
13. Crowther, R. A., Daniel, S. E., and Goedert, M. (2000) *Neurosci. Lett.* **292,** 128–130
14. Biere, A. L., Wood, S. J., Wypych, J., Steavenson, S., Jiang, Y., Anafi, D., Jacobsen, F. W., Jarosinski, M. A., Wu, G.-M., Louis, J.-C., Martin, F., Nahri, L. O., and Citron, M. (2000) *J. Biol. Chem.* **275,** 34574–34579
15. Serpell, L. C., Berriman, J., Jakes, R., Goedert, M., and Crowther, R. A. (2000) *Proc. Natl. Acad. Sci. U. S. A.* **97,** 4897–4902
16. Narhi, L., Wood, S. J., Steavenson, S., Jiang, Y., Wu, G. M., Anafi, D., Kaufman, S. A., Martin, F., Sitney, K., Denis, P., Louis, J.-C., Wypych, J., Biere, A. L., and Citron, M. (1999) *J. Biol. Chem.* **274,** 9843–9846
17. Conway, K. A., Harper, J. D., Lansbury, P. T. (1998) *Nat. Med.* **4,** 1318–1320
18. El-Agnaf, O. M. A., Jakes, R., Curran, M. D., Wallace, A. (1998) *FEBS Lett.* **440,** 67–70
19. Conway, K. A., Lee, S.-J., Rochet, J.-C., Ding, T. T., Williamson, R. E., and Lansbury, P. T. (2000) *Proc. Natl. Acad. Sci. U. S. A.* **97,** 571–576
20. Conway, K. A., Harper, J. D., and Lansbury, P. T. (2000) *Biochemistry* **39,** 2552–2563
21. McLean, P., Kawamata, H., Ribich, S., and Hyman, B. T. (2000) *J. Biol. Chem.* **275,** 8812–8816
22. Jo, E., McLaurin, J., Yip, C. M., St. George-Hyslop, P., and Fraser, P. E. (2000) *J. Biol. Chem.* **275,** 34328–34334
23. Uversky, V. N., Li, J., and Fink, A. L. (2001) *J. Biol. Chem.* **276,** 10737–10744
24. Giasson, B. I., Murray, I. V. J., Trojanowski, J. Q., and Lee, V. M.-Y. (2001) *J. Biol. Chem.* **276,** 2380–2386
25. Jakes, R., Crowther, R. A., Lee, V. M.-Y., Trojanowski, J. Q., Iwatsubo, T., and Goedert, M. (1999) *Neurosci. Lett.* **269,** 13–16
26. Lippa, C. F., Fujiwara, H., Mann, D. M. A., Giasson, B., Baba, M., Schmidt, M. L., Nee, L. E., O'Connell, B., Pollen, D. A., St. George-Hyslop, P., Ghetti, B., Nochlin, D., Bird, T. D., Cairns, N. J., Lee, V. M.-Y., Iwatsubo, T., and Trojanowski, J. Q. (1998) *Am. J. Pathol.* **153,** 1365–1370
27. Culvenor, J. G., McLean, C. A., Cutt, S., Campbell, B. C. V., Maher, F., Jäkälä, P., Hartmann, T., Beyreuther, K., Masters, C. L., and Li, Q.-X. (1999) *Am. J. Pathol.* **155,** 1173–1181
28. Jakes, R., Spillantini, M. G., and Goedert, M. (1994) *FEBS Lett.* **345,** 27–32
29. Hasegawa, M., Watanabe, A., Takio, K., Suzuki, M., Arai, T., Titani, K., and Ihara, Y. (1993) *J. Neurochem.* **60,** 2068–2077
30. Fujiwara, H., Hasegawa, M., Dohmae, N., Kawashima, A., Masliah, E., Goldberg, M. S., Shen, J., Takio, K., and Iwatsubo, T. (2002) *Nat. Cell Biol.* **4,** 160–164
31. Goedert, M., Jakes, R., Spillantini, M. G., Hasegawa, M., Smith, M. J., and Crowther, R. A. (1996) *Nature* **383,** 550–553
32. Crowther, R. A., Olesen, O. F., Jakes, R., and Goedert, M. (1992) *FEBS Lett.* **309,** 199–202
33. Wille, H., Drewes, G., Biernat, J., Mandelkow, E.-M., and Mandelkow, E. (1992) *J. Cell Biol.* **118,** 573–584
34. Novak, M., Kabat, J., and Wischik, C. M. (1993) *EMBO J.* **12,** 365–370
35. Ksiezak-Reding, H., and Yen, S.-H. (1991) *Neuron* **6,** 717–728

ELSEVIER

Neuroscience Letters 341 (2003) 74–78

Neuroscience Letters

www.elsevier.com/locate/neulet

Proteolytic cleavage and cellular toxicity of the human α1A calcium channel in spinocerebellar ataxia type 6

Takayuki Kubodera[a,b,1], Takanori Yokota[a,1], Kiyoshi Ohwada[a], Kinya Ishikawa[a], Hiroyuki Miura[b], Takeshi Matsuoka[b], Hidehiro Mizusawa[a,*]

[a]*Department of Neurology and Neurological Science, Graduate School of Medicine, Tokyo Medical and Dental University, 1-5-45 Yushima, Bunkyo-ku, Tokyo 113-8519, Japan*

[b]*Fifth Department of Internal Medicine, Tokyo Medical University, 3-20-1 Chuou, Ami-machi, Inashiki-gun, Ibaraki 300-0395, Japan*

Received 12 December 2002; received in revised form 22 January 2003; accepted 24 January 2003

Abstract

Spinocerebellar ataxia type 6 (SCA6) is a neurodegenerative disease caused by small CAG repeat expansion in the α1A calcium channel gene. We found that the human α1A calcium channel protein expressed in human embryonic kidney 293T cells produces a 75 kDa C-terminal fragment. This fragment is more toxic to cells than the full-length α1A calcium channel, regardless of polyglutamine tract length. In cells stably transfected with plasmids of full-length α1A calcium channel cDNAs, the C-terminal fragment protein is present in the mutant transformant but not in the wild-type one, indicative that this C-terminal fragment with the expanded polyglutamine tract is more resistant to proteolysis than that with the normal sized polyglutamine tract. We speculate that the toxic C-terminal fragment, in which resistance to proteolysis is rendered by the expanded polyglutamine, has a key role in the pathological mechanism of SCA6.

Keywords: Spinocerebellar ataxia type 6; α1A voltage-dependent calcium channel; Polyglutamine disease; Proteolytic cleavage; Cellular toxicity

Spinocerebellar ataxia type 6 (SCA6) is a dominantly inherited neurodegenerative disease characterized by progressive ataxia and dyasrthria caused by cerebellar atrophy. The underlying mutation in SCA6 is an expansion of the trinucleotide CAG repeat in exon 47 of the *CACNA1A* gene which encodes the α1A subunit of the P/Q type voltage-dependent calcium channel [13]. Unlike such other polyglutamine diseases as Huntington's disease (HD), Machado–Joseph disease (MJD), and dentatorubral-pallidoluysian atrophy (DRPLA) the expanded SCA6 alleles unusually have small expansions (21–30 repeats compared to generally >40 repeats in other polyglutamine diseases) [13]. SCA6, therefore, is considered to have a cell death mechanism that differs from other polyglutamine diseases.

We found that the full-length α1A calcium channel expressed in cultured cells is processed, and a C-terminal polyglutamine-containing fragment which is less soluble and more toxic than the truncated polyglutamine stretch itself is produced. Interestingly, the expanded polyglutamine of the C-terminal fragment is not itself toxic, rather it increases the toxic fragment's resistance to proteolysis. We propose that there is a gain of toxicity in polyglutamine disease which is related to, but not directly caused by, the expanded polyglutamine.

The construction of full-length human *CACNA1A* cDNAs with 13 (normal range) or 28 (expanded) CAG repeats was reported previously (respectively, pFL-Q13 and pFL-Q28) [8]. Human embryonic kidney (HEK) 293T cells were either transiently or stably transfected. The cells do not express an endogenous α1A calcium channel. Transfection was done with GenePORTER (Gene Therapy Systems) according to the manufacturer's protocol. Transfected cells were cultured in the presence of 400 μg/ml G418 (Sigma), after which G418-resistant cells were selected and subcloned to establish a stable cell line. Reverse transcription-polymerase chain reaction (RT-PCR) was used to screen for *CACNA1A* mRNA expression of stably transfected cells. Total RNA was extracted from these cells, and RT-PCR of the CAG repeat sequence of the *CACNA1A* mRNA performed as described previously [8].

* Corresponding author. Tel.: +81-3-5803-5233; fax: +81-3-5803-0134.
E-mail address: h-mizusawa.nuro@tmd.ac.jp (H. Mizusawa).
[1] These authors contributed equally to this work.

0304-3940/03/$ - see front matter © 2003 Elsevier Science Ireland Ltd. All rights reserved.
doi:10.1016/S0304-3940(03)00156-3

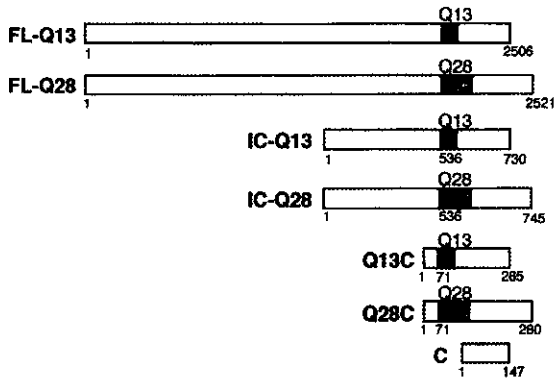

Fig. 1. Structures of full-length and truncated *CACNA1A* cDNA expression constructs. pFL-Q13, -Q28: full-length wild-type, and mutant *CACNA1A* cDNA construct (with 13 or 28 CAG repeats); pIC-Q13, -Q28, pQ13C, -Q28C: 5′-sequence deleted construct with 13 or 28 CAG repeats; pC: 3′-end construct without CAG repeats. Open reading frames are boxed and polyglutamine tracts hatched. Numbers below each box show the amino acid position counted from the initiation site of each construct.

For Western blotting, at 48 h post-transfection, cells were solubilized in non-denaturing lysis buffer (50 mM Tris–HCl, 150 mM Nacl, 1% Triton X-100, 10% grycelol) and detergent-soluble/insoluble fractionation was done by previously described method [7]. The insoluble pellet was solubilized in sodium dodecyl sulfate (SDS) (final concentration 4%). Equal sample volumes from the soluble and insoluble fractions were separated on 5–15% gradient SDS-polyacrylamide gels, immunoblotted with rabbit polyclonal antibody specific for the C-terminal portion of the α1A calcium channel protein (A6PRT-C) or with anti-myc antibody (Santa Cruz), then made visible by enhanced chemiluminescence (Amersham Pharmacia).

Cell viability was assessed by measuring luciferase activity, and the cell death rate by trypan blue exclusion. HEK 293T cells were plated in 6-well plates at 1×10^5 cells/cm^2 density, and 1 μg of the full-length or truncated *CACNA1A* cDNA construct was co-transfected with 0.1 μg of pGL3-Control Vector (encoding luciferase, Promega) and 0.1 μg of pEGFP-C2 (encoding green fluorescent protein, Clontech) by GenePORTER. At 48 h post-transfection, cells were harvested to measure luciferase activity. Luciferase activities were measured by Luciferase Aassay System (Promega) according to the manufacturer's protocol. At the same time, cells were incubated in trypan blue solution and the number nonviable (blue) cells recorded. Statistical analyses were done with Student's *t*-test and *P*-values less than 0.05 were considered statistically significant.

HEK 293T cells were transiently transfected with full-length human *CACNA1A* cDNAs containing 13 (normal range) or 28 (expanded) CAG repeats. Western blot analysis with A6PRT-C antibody showed a band at about 280 kDa (arrowhead) that represented the intact, full-length calcium channel (Fig. 2, lanes FL-Q13 and FL-Q28). In addition to the full-length α1A calcium channel, a prominent band migrating at about 75 kDa (arrow) was detected in both the cell lysates transfected with pFL-Q13 and -Q28, the pFL-Q28 product migrated slightly slower than pFL-Q13 product. This 75 kDa product should be the C-terminal portion of the α1A calcium channel because the difference in its molecular weight in FL-Q13 and FL-Q28 is

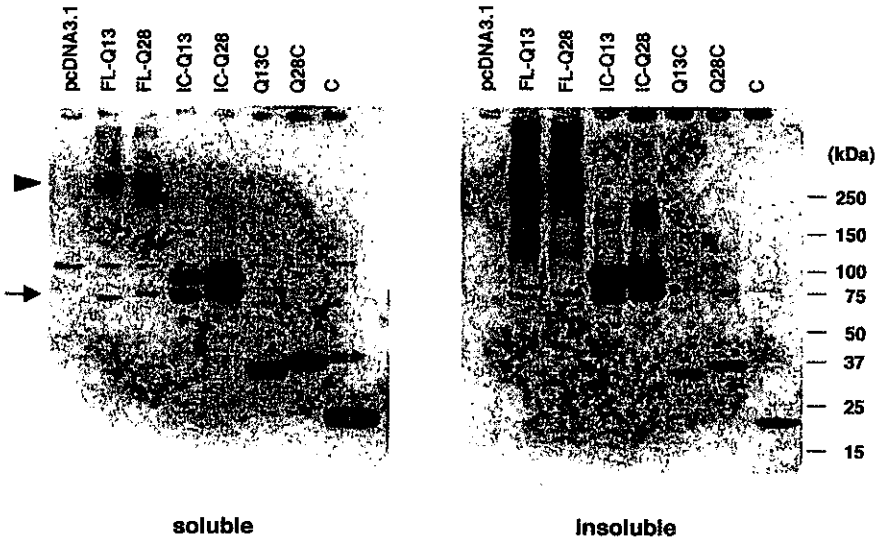

Fig. 2. Western blot of cells transfected transiently with full-length or truncated *CACNA1A* cDNA constructs by anti-calcium channel antibody (A6PRT-C). Cell lysates were fractionated into 1% Triton X-soluble or -insoluble fractions. Bands of each expressed protein are present at the expected sizes. The upper band, migrating at the molecular weight of about 280 kDa (arrowhead) is the full-length α1A calcium channel protein, and that at about 75 kDa (arrow) is the C-terminal cleavage fragment containing the polyglutamine tract. In the IC-Q13 and -Q28 lanes, C-terminal fragments are present at the sites at which FL-Q13 and -Q28 are cleaved. In the FL and IC samples, the amount of the insoluble fraction was greater than that of the soluble one.

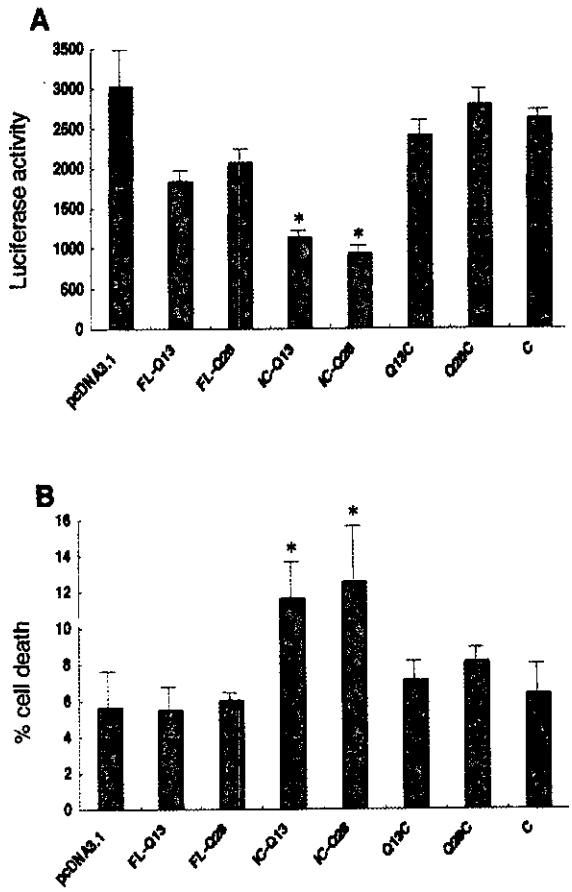

Fig. 3. Toxicity tests of cells transfected transiently with full-length or truncated constructs. (A) Luciferase activity 48 h after transfection with the indicated *CACNA1A* cDNA constructs and pcDNA3.1(+) control plasmid. Cells transfected with pIC-Q13 and -Q28 had lower luciferase activities than those transfected with control. (B) Cell toxicity shown by trypan blue exclusion after transient transfection with each construct. Cell death increased significantly in cells transfected with pIC-Q13 and -Q28, but the difference between them was not marked. Cellular toxicity based on trypan blue exclusion was consistent with luciferase activity measurements. Values are means plus SEM.

compatible with the difference in the molecular weight sizes of the wild-type's and mutant's polyglutamine tract lengths. Moreover, HEK 293T cells were transfected with constructs (myc-pFL-Q13 or -Q28) tagged with myc at the C-terminal, and anti-myc antibody recognized a band corresponding to the 75 kDa band (data not shown). Based on the molecular weight size of the C-terminal fragment, the cleavage site should be downstream of domain IV of the α1A calcium channel. This cleavage fragment corresponds to the C-terminal intracellular cytoplasmic region of the protein.

Various truncated constructs of *CACNA1A* cDNAs were generated to investigate whether expression of the full-length or truncated α1A calcium channel protein causes cellular toxicity (Fig. 1). Truncated constructs (pIC, pQ, pC) were prepared by removing the 5′-region of pFL and inserting an oligomer carrying the Kozak consensus sequence and an ATG start codon into the 5′-deleted plasmid. pIC encodes the C-terminal intracellular cytoplasmic region of the calcium channel and the translated protein carries the 75 kDa cleavage product. pQ encodes more of the truncated C-terminal portion with the polyglutamine tract. pC encodes the sequence downstream of the polyglutamine tract. Western blot analysis showed that each construct produced signals in the predicted positions (Fig. 2). Cell lysates from pIC transfections also showed signals that migrated at 75 kDa, suggesting that IC is cleaved at the site at which the full-length α1A calcium channel is cleaved. More Q13C, Q28C and C fragments were present in the soluble than insoluble fraction, whereas full-length proteins and IC fragments were more observed in the insoluble fraction. The 75 kDa band densities in the FL-Q13 and -Q28, and in the IC-Q13 and IC-Q28 lysates did not differ much, evidence that the length of the polyglutamine tract did not change the cleavage profile of the α1A calcium channel protein.

On cellular toxicity tests, only the pIC-Q13 and pIC-Q28 constructs were toxic to cells (Fig. 3A,B). Unexpectedly there was no marked difference in transfection with pIC constructs that expressed the normal sized (pIC-Q13) or the expanded polyglutamine tract (pIC-Q28). As compared to mock transfection results, no pFL, pQ or pC construct showed cellular toxicity.

The toxicities of pIC-Q13 and pIC-Q28 were enhanced after treatment with proteasome inhibitor, 10 μM lactacystin, for 24 h; ratio of luciferase activities of pIC-Q13 and pIC-Q28 constructs to that of mock transfection as a viability index were decreased by 33 and 34% after lactacystin treatment, respectively.

HEK 293T cells were stably transfected with constructs of the full-length *CACNA1A* cDNA containing 13 or 28 repeats fused with GFP at the 5′-terminal (GFP-FL13 and GFP-FL28, respectively). Six of the GFP-FL13- and two of the GFP-FL28- expressing clones were selected by GFP fluorescence and RT-PCR analysis of the CAG repeat sequence (data not shown). Western blot analysis results of stably transfected cells with antibody A6PRT-C are shown in Fig. 4. No obvious full-length α1A calcium channel was present in the GFP-FL13 and GFP-FL28 cell lines. There was a clear band migrating at about 75 kDa only in the GFP-FL28 cell line (arrow). In SDS-PAGE this fragment protein is located at the same position as the C-terminal cleavage fragment of HEK 293T cells transiently transfected with pFL-Q28.

In such other polyglutamine diseases as HD, MJD and DRPLA mutant proteins, which are expressed not as part of the entire protein but part of the polyglutamine-containing fragment, aggregate and trigger cell death in cultured cells [5,6,9]. Similarly, in our study of SCA6, expression of the C-terminal fragment with a polyglutamine tract was more toxic to cultured cells than was the mutant full-length

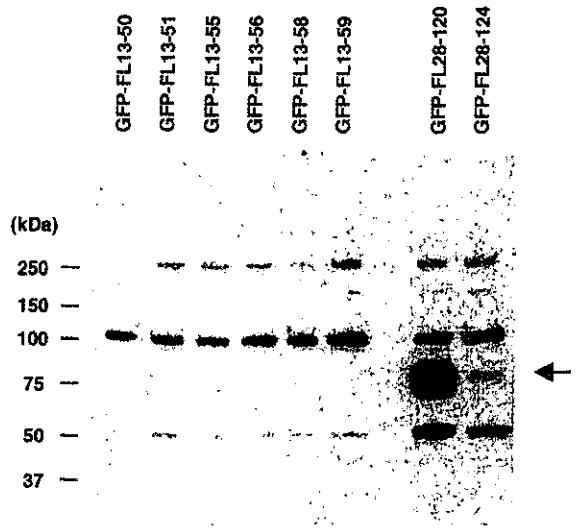

Fig. 4. Western blot of cells transfected stably with GFP-α1A calcium channel fusion protein expression constructs by antibody A6PRT-C. Six cell lines express GFP-FL-13, and the other two express GFP-FL-28. No full-length α1A calcium channel protein is present in the GFP-FL-13 or GFP-FL-28 cell line, and the 75 kDa protein is present only in the GFP-FL-28 cell line.

calcium channel. Toxicity of the C-terminal fragment, however, did not depend on polyglutamine length. Moreover, the C-terminal fragment is less soluble and more toxic to cultured cells than the more truncated protein with just the polyglutamine stretch, and the polyglutamine stretch itself did not have cellular toxicity when compared with the control. This lack of toxicity by the truncated polyglutamine of calcium channel is not surprising because the expanded CAG repeat number of SCA6 is still within the normal repeat number range of other polyglutamine diseases. We speculate that SCA6 differs from the other polyglutamine diseases in that the processed polyglutamine-containing fragment is toxic but its toxicity is not directly caused by the polyglutamine stretch.

There was no marked difference in the cellular toxicity between the constructs with normal and expanded CAG repeats. If C-terminal fragment toxicity is responsible for cell death, how does the length of polyglutamine determine the phenotype? Findings for stable cell lines should provide important clues to the answer of this question. Western blotting of stably transfected cells detected no mutant or wild-type full-length calcium channel and the 75 kDa fragment was present only in the mutant transformant. This finding suggests that the full-length calcium channel has a low expression level or rapidly degenerates in the stable cell lines. In contrast, the processed C-terminal fragment with the expanded polyglutamine tract, but not that with the normal sized polyglutamine tract, is resistant to proteolysis and accumulates. Because HEK 293T cells do not have an endogenous β or α2/δ component, necessary for assembling a calcium channel with an α1A component, the localization and circumstances of the α1A component expressed in cultured cells is not the same as in vivo, and its processing may differ. Here, we speculate that increased resistance of the mutant C-terminal fragment to proteolysis than wild-type would explain the phenotype of neurodegeneration in SCA6, but further evidence needs to be demonstrated to prove this hypothesis.

Loss of disease protein function has been suggested to be related to the phenotype of polyglutamine diseases in recent reports [1,3]. Various lines of evidence, however, show that mutant proteins with an expanded polyglutamine stretch, when cleaved, gain toxic function [2,4,6,9,11]. The expanded polyglutamine itself is considered to become toxic due to conformational change [10,12]. Our hypothesis differs in that the expanded polyglutamine itself in SCA6 does not have toxicity, rather it causes the persistence of toxic fragments. This would can explain why the small CAG repeat expansion in SCA6 can induce cell death.

References

[1] E. Cattaneo, D. Rigamonti, D. Goffredo, C. Zuccato, F. Squitieri, S. Sipione, Loss of normal huntingtin function: new developments in Huntington's disease research, Trends Neurosci. 24 (2001) 182–188.

[2] M. DiFiglia, E. Sapp, K.O. Chase, S.W. Davies, G.P. Bates, J.P. Vonsattel, N. Aronin, Aggregation of huntingtin in neuronal intranuclear inclusions and dystrophic neuritis in brain, Science 277 (1997) 1990–1993.

[3] I. Dragatsis, M.S. Levine, S. Zeitlin, Inactivation of Hdh in the brain and testis results in progressive neurodegeneration and sterility in mice, Nat. Genet. 26 (2000) 300–306.

[4] Y.P. Goldberg, D.W. Nicholson, D.M. Rasper, M.A. Kalchman, H.B. Koide, R.K. Graham, M. Bromm, P. Kazemi-Esfarjani, N.A. Thornberry, J.P. Vaillancourt, M.R. Hayden, Cleavage of huntingtin by apopain, a proapoptotic cysteine protease, is modulated by the polyglutamine tract, Nat. Genet. 13 (1996) 442–449.

[5] S. Igarashi, R. Koide, T. Shimohata, M. Yamada, Y. Hayashi, H. Takano, H. Date, M. Oyake, T. Sato, A. Sato, S. Egawa, T. Ikeuchi, H. Tanaka, R. Nakano, K. Tanaka, I. Hozumi, T. Inuzuka, H. Takahashi, S. Tsuji, Suppression of aggregate formation and apoptosis by transglutaminase inhibitors in cells expressing truncated DRPLA protein with an expanded polyglutamine stretch, Nat. Genet. 18 (1998) 111–117.

[6] H. Ikeda, M. Yamaguchi, S. Sugai, Y. Aze, S. Narumiya, A. Kakizuka, Expanded polyglutamine in the Machado-Joseph disease protein induces cell death in vitro and in vivo, Nat. Genet. 13 (1996) 196–202.

[7] Y. Imai, M. Soda, H. Inoue, N. Hattori, Y. Mizuno, R. Takahashi, An unfolded putative transmembrane polypeptide, which can lead to endoplasmic reticulum stress, is a substrate of Parkin, Cell 105 (2001) 891–902.

[8] K. Ishikawa, H. Fujigasaki, H. Saegusa, K. Ohwada, T. Fujita, H. Iwamoto, Y. Komatsuzaki, S. Toru, H. Toriyama, M. Watanabe, N. Ohkoshi, S. Shoji, I. Kanazawa, T. Tanabe, H. Mizusawa, Abundant expression and cytoplasmic aggregations of α1A voltage-dependent calcium channel protein associated with neurodegeneration in spinocellebellar ataxia type 6, Hum. Mol. Genet. 8 (1999) 1185–1193.

[9] D. Martindale, A. Hackam, A. Wieczorek, L. Ellerby, C. Wellington, K. McCutcheon, R. Singaraja, P. Kazemi-Esfarjani, R. Devon, S.U.

Kim, D.E. Bredesen, F. Tufaro, M.R. Hayden, Length of huntingtin and its polyglutamine tract influences localization and frequency of intracellular aggregates, Nat. Genet. 18 (1998) 150–154.
[10] H.L. Paulson, N.M. Bonini, K.A. Roth, Polyglutamine disease and neuronal cell death, Proc. Natl. Acad. Sci. USA 97 (2000) 12957–12958.
[11] G. Schilling, J.D. Wood, K. Duan, H.H. Slunt, V. Gonzales, M. Yamada, J.K. Cooper, R.L. Margolis, N.A. Jenkins, N.G. Copeland, H. Takahashi, S. Tsuji, D.L. Price, D.R. Borchelt, C.A. Ross, Nuclear accumulation of truncated atrophin-1 fragments in a transgenic mouse model of DRPLA, Neuron 24 (1999) 275–286.
[12] J.P. Taylor, J. Hardy, K.H. Fischbeck, Toxic proteins in neurodegenerative disease, Science 296 (2002) 1991–1995.
[13] O. Zhuchenko, J. Bailey, P. Bonnen, T. Ashizawa, D.W. Stockton, C. Amos, W.B. Dobyns, S.H. Subramony, H.Y. Zoghbi, C.C. Lee, Autosomal dominant cerebellar ataxia (SCA6) associated with small expansions in the α1A-voltage-dependent calcium cgannel, Nat. Genet. 15 (1997) 62–69.

J Hum Genet (2003) 48:111–118

ORIGINAL ARTICLE

Mingshun Li · Kinya Ishikawa · Shuta Toru
Hiroyuki Tomimitsu · Minoru Takashima · Jun Goto
Yoshihisa Takiyama · Hidenao Sasaki · Issei Imoto
Johji Inazawa · Tatsushi Toda · Ichiro Kanazawa
Hidehiro Mizusawa

Physical map and haplotype analysis of 16q-linked autosomal dominant cerebellar ataxia (ADCA) type III in Japan

Received: June 25, 2002 / Accepted: November 22, 2002

Abstract Autosomal dominant cerebellar ataxia (ADCA) is a group of heterogeneous neurodegenerative disorders. We previously mapped a gene locus for ADCA with pure cerebellar syndrome (ADCA type III) to a 3-cM region in chromosome 16q, and found a common haplotype among affected individuals. This region was exactly within the locus for another ADCA, spinocerebellar ataxia type 4 (SCA4). To identify the gene causing 16q-linked ADCA type III, we constructed a contig with 38 bacterial artificial chromosome clones between D16S3043 and D16S3095. The size of this contig was estimated to be 4.8 Mb. We found more than 500 nucleotide tandem repeats, including 9 CAG/CTG repeats in this candidate region, although none of the 94 tandem repeats analyzed were expanded in affected individuals. However, we found 11 new polymorphic markers, giving 22 markers spanning the candidate region. By typing these markers on eight Japanese families with ADCA type III, including two new families, we found that a common "founder" haplotype is seen in a more restricted 3.8-Mb region, spanning markers GGAA05 and D16S3095. We present here a newly refined critical interval of 16q-ADCA type III/SCA4. Data of 11 new DNA markers on 16q22.1 would also be useful for other research of genes mapped to this region.

Key words Autosomal dominant cerebellar ataxia type III (ADCA type III) · Spinocerebellar ataxia type 4 (SCA4) · 16q22.1 · Physical map · Bacterial artificial chromosome (BAC) contig · Haplotype analysis

M. Li · K. Ishikawa · S. Toru · H. Tomimitsu · M. Takashima · H. Mizusawa (✉)
Department of Neurology and Neurological Science, Graduate School of Medical and Dental Sciences, Tokyo Medical and Dental University, 1-5-45 Yushima, Bunkyo-ku, Tokyo 113-8519, Japan
Tel. +81-3-5803-5233; Fax +81-3-5803-0134
e-mail: h-mizusawa.nuro@tmd.ac.jp

S. Toru
Japan Health Sciences Foundation, Tokyo, Japan

J. Goto · I. Kanazawa
Department of Neurology, Division of Neuroscience, Graduate School of Medicine, University of Tokyo, Tokyo, Japan

Y. Takiyama
Department of Neurology, Jichi Medical School, Tochigi, Japan

H. Sasaki
Department of Neurology, Hokkaido University School of Medicine, Sapporo, Japan

I. Imoto · J. Inazawa
Department of Molecular Cytogenetics, Medical Research Institute, Tokyo Medical and Dental University, Tokyo, Japan

T. Toda
Division of Functional Genomics, Department of Post-Genomics and Diseases, Course of Advanced Medicine, Osaka University Graduate School of Medicine, Suita, Japan

Introduction

Autosomal dominant cerebellar ataxia (ADCA) is a group of heterogeneous neurodegenerative disorders (Harding 1982). It is clinically characterized by progressive cerebellar ataxia, although other extracerebellar signs, such as pyramidal or extrapyramidal signs, ophthalmoparesis, amyotrophy, and peripheral neuropathy may be variably present. ADCA is classified into three types on the basis of its clinical features (Harding 1982). ADCA types I and II are clinically characterized by prominent extracerebellar signs and macular dystrophy, respectively. In contrast, ADCA type III is characterized by purely cerebellar ataxia throughout the course of illness (Harding 1982; Ishikawa et al. 1996).

At present, 18 loci have been reported to be responsible for ADCA, although there are still other families that do not map to any of these loci. Among these disorders, causative genes have been further identified as expansions of a trinucleotide (CAG) repeat for SCA1 (Orr et al. 1993), SCA2 (Imbert et al. 1996; Sanpei et al. 1996), Machado-Joseph disease/SCA3 (Kawaguchi et al. 1994), SCA6 (Zhuchenko et al. 1997), SCA7 (David et al. 1997), SCA12 (Holmes et al. 1999), SCA17 (Koide et al. 1999; Nakamura et al. 2001) and dentatorubral and pallidoluysian atrophy (DRPLA) (Nagafuchi et al. 1994). Spinocerebellar ataxia type 8 has been proposed to be caused by the expansion of

a CTG repeat in the 3′ noncoding region of the SCA8 gene (Koob et al. 1999), and the SCA10 mutation has been demonstrated to be the expansion of the pentanucleotide ATTCT repeat in an intron of this gene (Matsuura et al. 2000). Only the gene loci have been identified for the remaining 8 SCAs: SCA4 on 16q22.1 (Gardner et al. 1994; Flanigan et al. 1996), SCA5 on 11 cen (Ranum et al. 1994), SCA11 on 15q14–q21.3 (Worth et al. 1999), SCA13 on 19q13.3–q13.4 (Herman-Bert et al. 2000), SCA14 on 19q13.4–q ter (Yamashita et al. 2000), SCA16 on 8q22.1–q24.1 (Miyoshi et al. 2001), SCA19 (Verbeek et al. 2002), and SCA21 (Vuillaume et al. 2002).

We previously mapped a gene responsible for ADCA type III to chromosome 16q (Nagaoka et al. 2000). The region spans a 10.9-cM region flanked by D16S3089 and D16S515, the locus identical to the SCA4 locus (Gardner et al. 1994; Flanigan et al. 1996). We further identified that our "16q-linked ADCA type III" has a common founder haplotype for markers between D16S3043 and D16S3095 in this region (Takashima et al. 2001).

To identify the causative gene mutation for 16q-linked ADCA type III, we first constructed a physical map spanning D16S3043 and D16S3095 because no complete physical maps had been available. We found 11 new polymorphic markers in this region. Using these markers, we analyzed the haplotype of eight families and narrowed the critical region.

We searched tandem repeats in this candidate region for any abnormal expansion in our patients, because expansions of certain repeat sequences, such as CAG/CTG or ATTCT repeats, are the only causative mutations for SCAs.

Here we show a complete bacterial artificial chromosome (BAC) contig of the locus for 16q-linked ADCA type III, information of newly developed markers in this region, and results of haplotype analysis.

Patients and methods

Patients and families

Eight families were studied, six of which have been previously described (Ishikawa et al. 1996; Nagaoka et al. 2000; Takashima et al. 2001). Two other families have been included for the first time in this study because they also showed later-onset pure cerebellar ataxia with autosomal dominant inheritance (family trees are available on request). From our interviews with family members, we determined that these two families originated from the Tokyo Metropolitan area (T1) and the Gunma Prefecture (T2), indicating that none of our eight families are related.

Thirty-eight Japanese individuals whose family members have no history of neurodegenerative diseases were chosen as normal controls.

A peripheral blood sample was obtained with informed consent from each family member and control individual, and genomic DNA was extracted as previously described (Ishikawa et al. 1996).

Construction of the BAC contig

BAC clones were initially searched from National Center for Biotechnology Information (NCBI) genome sequencing contigs (http://www.ncbi.nlm.nih.gov/genome/seq) by microsatellite DNA markers linked to the critical interval. By this method, we obtained eight BAC clones, Rp11-123C5, Rp11-112G1, Rp11-361L15, Rp11-167P11, Rp11-292B23, Rp11-521L9, Rp11-502K10, and Rp11-311C24, from Research Genetics (Houtsville, AL, USA).

DNA from each BAC clone was extracted by a modified QIAGEN Plasmid Mini Purification Protocol (QIAGEN, Hilden, Germany). BAC clones were first confirmed to contain microsatellite DNA markers or Sequence targged site (STS) markers by polymerase chain reaction (PCR). These clones were then "end-sequenced" by T7 (5′-ATACGAC TCACTATA-3′) and Sp6 (5′-ATTTAGGTGACACTA TA-3′) primers.

We then browsed for sequences of BAC clones in BLASTN (http://www.ncbi.nlm.nih.gov/BLAST/) after eliminating repeat sequences using the RepeatMasker program (http://ftp.genome.washington.edu/cgi-bin/RepeatMasker), and, by repeating this method, we finally obtained five partial BAC contigs that nearly covered the entire candidate region. Four small remaining gaps were filled with six BAC clones by browsing databases: Ensembl Map view (http://www.ensembl.org/perl/mapview?chr=16), HGREP (http://hgrep.ims.u-tokyo.ac.jp/cgi-bin/HTG_tool/view.cgi), and TIGR (http://www.tigr.org/tdb/humgen/bac_end_search/bac_end_intro.htm/).

Sequencing

Sequencing reactions were performed using the ABI PRISM BigDye Terminator Cycle Sequencing Ready Reaction kit (PE Applied Biosystems, Foster City, CA, USA). We cycle-sequenced 2–3 μg BAC DNA for 50 cycles with 6.4 pmol of either T7 or Sp6 primer on an ABI GeneAmp PCR system 9700 (PE Applied Biosystems).

For genomic DNA, 10 ng PCR product was cycle-sequenced for 25 cycles with 3.2 pmol of each primer. Nucleotide sequences were analyzed on an ABI PRISM 377 DNA Sequencer (PE Applied Biosystems).

Searching nucleotide-repeat variation

We derived the BAC clone sequence from NCBI (http://www.ncbi.nlm.nih.gov/entrez). To identify tandem repeats, namely, 2 (di-), 3 (tri-), 4 (tetra-), 5 (penta-), and 6 (hexa-) tandem repeats, we used the RepeatMasker program. Oligonucleotide primers were then designed to amplify the genomic DNA segment flanking each repeat. PCR was performed in a final volume of 20 μl, containing 10 ng of genomic DNA, 3.4 pmol of each primer, 2.5 mM each of deoxyribonucleoside triphosphates, and 0.75 unit of Taq polymerase (Takara, Tokyo, Japan) or Gold Taq polymerase (Applied Biosystems Ampli-Taq Gold with Gene Amp).

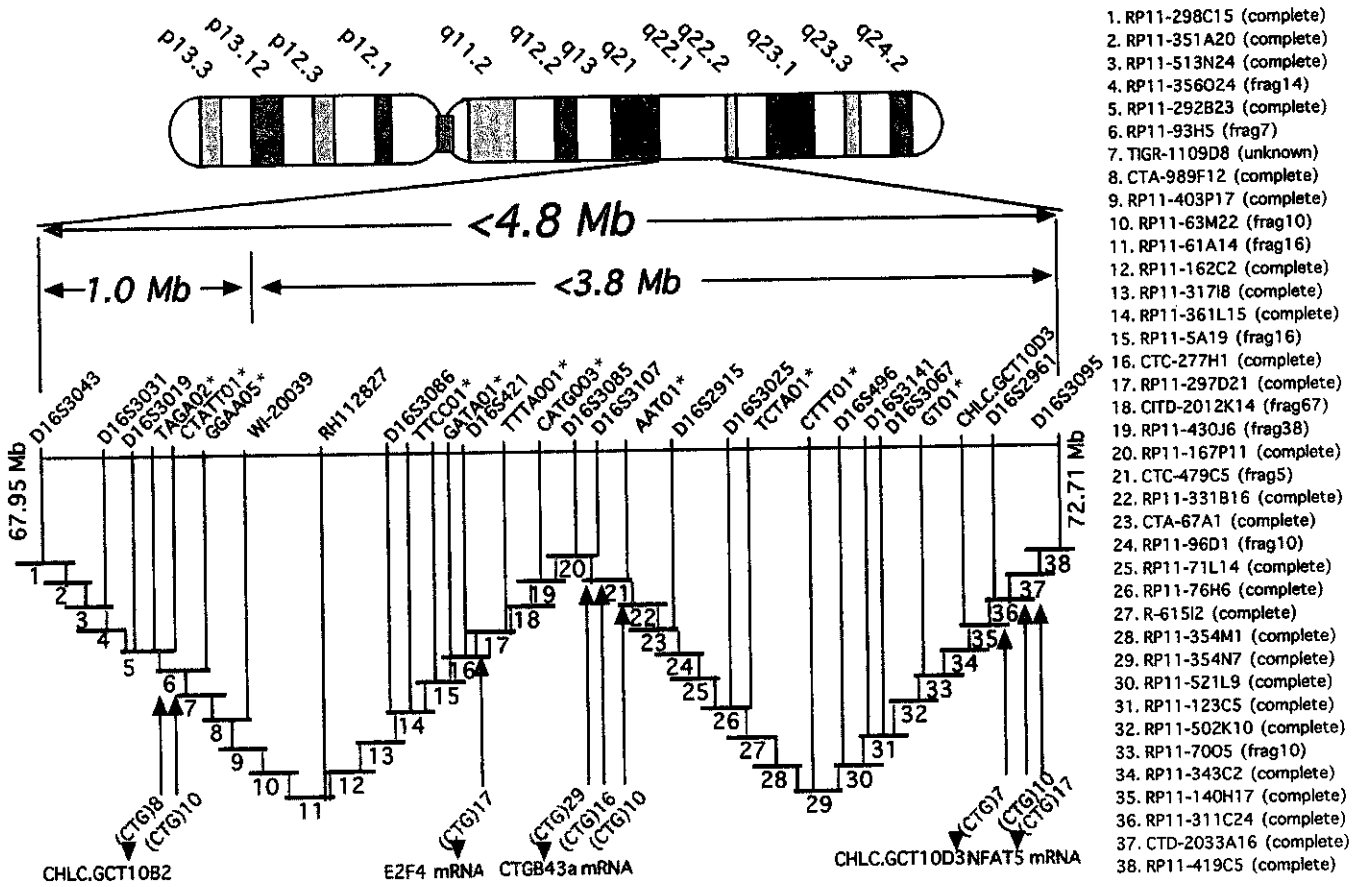

Fig. 1. The physical map of the candidate region of 16q-linked autosomal dominant cerebellar ataxia (ADCA) type III. The size of this bacterial artificial chromosome (BAC) contig was estimated to be no more than 4.8 Mb, with 38 BAC clones spanning the centromeric marker D16S3043 (shown on the *left*) and the telomeric marker D16S3095 (shown on the *right*). The identification of each BAC clone and the most up-to-date sequence status of each clone [i.e., completely sequenced or still in numbers of fragments (*frag*)] are shown on the *right*. *Shaded lines* between BAC clones indicate that the connection of the two BAC clones was confirmed by end sequences, and *bold lines* indicate that the connection was confirmed from database searches. The sequence of BAC clone TIGR-1109D8 is unknown. BAC Rp11-93H5, CTC277H1, CTC479C5, Rp11-331B16, Rp11-140H17, and Rp11-311C24 contain (CAG/CTG)n repeats. The locations of 11 newly identified polymorphic markers are indicated with *asterisks*. The new founder haplotype region is no more than 3.8 Mb between GGAA05 and D16S3095

The PCR products were separated on 2% agarose gel. To precisely genotype each DNA sample, we labeled the 5′ end of the forward primer with fluorescent isothiocyanate, and amplified it. PCR products were separated on the Automated DNA Sequencer II (ALF, Pharmacia Biotech, Umea, Sweden) and analyzed with ALF Win Manager as previously described (Ishikawa et al., 1996; Ishikawa et al. 1997). Eleven new markers with the highest polymorphism were then selected for genotyping and analysis for association with disease.

Haplotype analysis and linkage disequilibrium

Haplotype analysis was performed with 22 markers, including the 11 new markers, that showed enough polymorphism: 16q cen-D16S3043, D16S3031, CTATT01, TAGA02, GGAA05, D16S3086, TTCC01, GATA01, D16S421, TTTA001, CATG003, D16S3085, D16S3107, AAT01, D16S3025, TCTA01, CTTT01, D16S496, D16S3067, D16S3141, GT01, and D16S3095 16q ter-, in the order shown on our physical map (Fig. 1). We analyzed genotypes of all available subjects, including those who married into these families. Because the 22 markers spaced in a distance of approximately 5 Mb, we reconstructed haplotypes in every family that showed minimum recombination events. The association of disease phenotype and each allele was statistically analyzed by Fisher's exact probability test.

Results

Construction of a BAC-based physical map contig

A complete contig spanning markers D16S3043 and D16S3095 was constructed with 38 BAC clones (Fig. 1). The size of this contig was estimated to be no more than 4.8 Mb from the database ENSEMBL. According to the most recent NCBI database, 25 of the 38 BAC clones (65%) have been completely sequenced. On the other hand, the sequence of one BAC clone, TIGR 1109D8, is unknown.

The remaining 12 BAC clones have some gaps in their sequences as of March 2002, although approximately 70% of their entire inserts have been published in a draft sequence version. Therefore, the nucleotide sequences of approximately 90% of the entire contig is now available.

According to the NCBI and ENSEMBL databases, at least 100 annotated genes are present within the candidate region, and 65 of them are expressed in the human brain.

Identification of repeat sequences

To search anonymous repeat sequences by RepeatMasker, we first had to know how powerful this software was in detecting tandem repeats. We inserted known tandem repeats with different repeat units in the known 6-kb nucleotide sequences, and applied the software program. By this test, we found that the software sufficiently detects dinucleotide repeats with more than nine repeat units, trinucleotide repeats with more than six repeat units, tetranucleotide repeats with more four repeat units, and penta- or hexanucleotide repeats with more than three repeat units (Table 1).

We next applied this software to each BAC contig and found 146 dinucleotide, 83 trinucleotide, 213 tetranucleotide, and 91 penta- or hexanucleotide repeats in the entire sequenced region (Table 2). These repeats were confirmed to be unique by checking the flanking sequences. This would indicate that there are more than 500 tandem repeats within the entire contig.

Table 1. RepeatMasker program detectable repeat units and selected repeat units in this study

	Detectable repeat units	Selected repeat units
Dinucleotide	>9	>19
Trinucleotide	>6	>6 (ATT/TAA>14)
Tetranucleotide	>4	>9
Pentanucleotide	>3	>4 (except ATTTT/TAAAA)
Hexanucleotide	>3	>4 (except ATTTTT/TAAAAA)

Identification of 11 new polymorphic markers in 16q22.1

Among approximately 500 tandem repeats, we first selected repeats with higher numbers of repeat units, because repeats with larger repeat units tend to be more polymorphic. From this context, we chose 14 dinucleotide repeats that have more than 19 repeat units (Table 1). Similarly, we chose 37 trinucleotide repeats that have more than 6 repeat units, except for ATT/TAA repeats; 32 tetranucleotide repeats with more than 9 repeat units; and 9 penta- or hexanucleotide repeats with more than 4 repeat units. For ATT/TAA repeats, we chose 2 repeats that have more than 14 repeat units. We examined whether these 94 markers were polymorphic.

When 38 normal Japanese individuals were genotyped, 26% of the tested repeats were demonstrated to be polymorphic: 12 dinucleotide, 1 trinucleotide, 10 tetranucleotide, and 1 pentanucleotide.

Among these 24 repeats, we selected the most polymorphic 11 repeats as "new" markers to analyze haplotypes in patients with ADCA type III (Tables 3, 4, 5). The sequences of primers of these 11 markers are described in Table 3, and the size of PCR products and allele frequencies among 38 control individuals are described in Table 4.

Haplotype and association analyses

Haplotypes of eight 16q-linked ADCA type III families are shown in Table 5. The P4 family from our previous study (Ishikawa et al. 1997; Nagaoka et al. 2000; Takashima et al. 2001) had the haplotype 3(316 bp)-5(194 bp)-6(260 bp), which was different from the haplotype of other

Table 2. Tandem repeats in the candidate region

Experimented/ total number	Types of repeats				
Dinucleotide 14/146	(CA/TG)n 11/100	(TA/AT)n 1/37	(GA/TC)n 2/9		
Trinucleotide 39/83	(CAG/GTC)n 9/9	(CGG/GCC)n 4/7	(CAA/GTT)n 16/24	(TAA/ATT)n 6/38	
	(ATG/TAC)n 0/1	(ACC/TGG)n 3/3	(TCC/AGG)n 1/1		
Tetranucleotide 32/213	(TTCC/GGAA)n 10/16	(TTCA/AAGT)n 6/14	(TAAA/ATTT)n 2/89	(TTTG/AAAC)n 0/42	(TGGA/ACCT)n 2/13
	(GGGT/CCCA)n 0/1	(CAAT/GTTA)n 1/6	(TCCC/AGGG)n 1/4	(TCTA/AGAT)n 1/3	
	(TTTC/AAAG)n 2/11	(CATA/GTAT)n 0/2	(TTAA/AATT)n 0/1	(ATAC/TATG)n 0/3	
	(CAGG/GTCC)n 1/1	(GATA/CTAT)n 3/3	(TGAA/ACTT)n 2/3	(CACG/GTGC)n 1/1	
Penta-, hexanucleotide 9/91	(TAAAA/ATTTT)n 1/25	(TTTTG/AAAAC)n 1/42	(TTTTC/AAAAG)n 0/8	(GTCTG/CAGAC)n 1/1	(CTATT/GATAA)n 1/1
	(GGGGT/CCCCA)n 1/4	(GGATG/CCTAC)n 1/1	(CGGGG/GCCCC)n 0/2	(GGATG/CCTAC)n 1/1	(GGGAGA)n 0/3
	(CATATA)n 1/1	(ATGGTG)n 1/2			

Table 3. New markers developed in this study

Marker name	Located BAC clone	Repeat	Primer sequence (5'-3')	Standard PCR product size (bp)
CTATT01	RP11-292B23	(CTATT)12	F:GGTGAGGATCTATCTAGATT R:GCCGCTGTGTGAATTAGAA	316
TAGA02	RP11-292B23	(TAGA)17	F:AGTGGGTAGAGGAGATGTTA R:GGGCAGAGAAAGAGTAACAA	194
GGAA05	RP11-93H5	(GA)6(GGGA)6(GGAA)13	F:GTTGCAGTGAGCGGAAATT R:CCTACCTCCAGTCCAGATT	244
TTCC01	RP11-361L15	(TTCC)23	F:CCATCTTATCTCTTAGTCCGT R:GTGAGCCAAGATCATGCCAT	168
GATA01	RP11-5A19	(GATA)16	F:GGGTCACTGAGATGTCCAGTA R:CGCTGTGAGCACTGCTCTCA	157
TTTA001	RP11-297D21	(TTTA)11	F:CCGAAATAGGCGTACCTAGGCTA R:AGTGAGCTGAGTTTGCACCACTG	218
CATG003	RP11-297D21	(CA)20	F:ACCACAGAGCTGAGGCCT R:AGCAAGTCTGCCTTGGAGAGG	192
ATT01	479C5	(ATT)15	F:CGAATCACAGACACACCCAC R:CAGAGATTGCAGTGAGCCAA	230
TCTA01	R-615I2	(TCTA)11	F:GGGAGGCAGTTTAATTCACTT R:GAGCGAGACTCCGTCTCAA	218
CTTT01	354N7	(CTTT)20	F:GCCCCAGATACGCCAGAG R:CCTCTCTACACTCCAGCCT	242
GT01	70O5	(GT)23	F:GGGCACTAAGGACACTTCTT R:GGCTCTGTCATCCATGTTATG	183

BAC, Bacterial artificial chromosome; PCR, polymerase chain reaction

families with the new markers CTATT01, TAGA02, and GGAA05, located in the centromeric region of the candidate interval. The new family T2 also had a different 2(244 bp) allele from other families for the marker GGAA05. However, all families had the same haplotype from the marker D16S3086 to the most telomeric marker GT01 (Table 5): 16 cen-D16S3086: allele 2-TTCC01: allele 4-GATA01: allele 2-D16S421: allele 3-TTTA001: allele 4-CATG003: allele 4-D16S3085: allele 2-D16S3107: allele 7-AAT01: allele 2-D16S3025: allele 4-TCTA01: allele 2-CTTT01: allele 8-D16S496: allele 5-D16S3067: allele 5-D16S3141: allele 3-GT01: allele 6–16q ter. This indicates that a new critical interval of this disease is a region between GGAA05 and D16S3095, no more than 3.8 Mb in size (Fig.1 and Table 5). Among 16 markers spaced in the new critical interval 10 showed significant association with the disease: TTCC01 ($P = 0.0462$), GATA01 ($P = 0.002$), D16S3107 ($P < 0.0001$), AAT01 ($P = 0.0258$), TCTA01 ($P = 0.0227$), CTTT01 ($P = 0.0009$), D16S496 ($P = 0.032$), D16S3067 ($P = 0.008$), D16S3141 ($P = 0.011$), and GT01 ($P < 0.0001$) (Table 5). In particular, three of these markers, D16S3107, CTTT01, and GT01, were in significant linkage disequilibrium (Tables 4, 5). In contrast, none of the 38 control individuals had the particular haplotype 2-4-2-3-4-4-2-7-2-4-2-8-5-5-3-6, indicating that this haplotype is significantly associated with the disease and may be useful for molecular diagnosis of 16q-ADCCA.

Screening of dynamic mutations in 16q-linked ADCA type III patients

In the entire sequenced region, we found nine CAG/CTG repeats that have more than seven repeat units by RepeatMasker (Fig. 1). Four of these were seen in the coding region of three genes, the E2F4 gene (Ginsberg et al. 1994), CTGB43a mRNA, and the NFAT5 gene (Lopez-Rodriguez et al. 1999; Hebinck et al. 2000). CAG repeats in *CTGB43a* and *NFAT5* encode polyglutamine tracts and a CAG repeat in *E2F4* is translated into a polyserine stretch. The other two CAG/CTG repeats have already been annotated as polymorphic CAG repeats in the Cooperative Human Linkage Center (CHLC) database (www.chlc.org). The remaining three CAG/CTG repeats, newly identified in this study, were not located in any known genes.

Amplifying these nine CAG/CTG repeats revealed that none of them were expanded in our patients with 16q-linked ADCA type III. Direct sequencing of the three genes, the E2F4 gene, CTGB43a mRNA, and the NFAT5 gene, disclosed that there are also no mutations in the coding regions of these genes.

Similarly, we tested 30 trinucleotide repeats, 32 tetranucleotide repeats, and 9 penta- or hexanucleotide repeats for polymorphism in control individuals (Table 2). However, we have so far not detected any abnormal expansions in 16q-linked ADCA type III patients.

Discussion

In the present study, we constructed a 4.8-Mb physical map consisting of 38 BAC clones covering the candidate region between D16S3043 and D16S3095 (Takashima et al. 2001). When we started constructing this contig, very few BAC or yeast artificial chromosome clones had been mapped to this region. In addition, the precise order of microsatellite DNA markers, used in examining the haplotype in our previous set of six families with ADCA type III, was not known (Dib et al. 1996; Takashima et al. 2001). By constructing the

Table 4. Size of PCR products and allele frequencies among control individuals on each newly developed DNA marker

Allele	CTATT01 (frequency)	TAGA02 (frequency)	GGAA05 (frequency)	TTCC01 (frequency)	GATA01 (frequency)	TTTA001 (frequency)	CATG003 (frequency)	AAAT01 (frequency)	TCTA01 (frequency)	CTTT01 (frequency)	GT01 (freuqnecy)
1	306 bp(0.014)	178 bp (0.094)	**240 bp (0.014)**	155 bp (0.013)	154 bp (0.191)	204 bp (0.05)	188 bp (0.064)	224 bp (0.012)	215 bp (0.013)	226 bp (0.025)	179 bp (0.026)
2	**311 bp (0.186)**	182 bp (0.014)	**244 bp (0.094)**	159 bp (0.026)	**158 bp (0.441)**	208 bp (0.025)	190 bp (0.013)	**230 bp (0.475)**	**219 bp (0.46)**	228 bp (0.036)	181 bp (0.171)
3	**316 bp (0.229)**	**186 bp (0.122)**	248 bp (0.149)	163 bp (0.08)	162 bp (0.294)	212 bp (0.275)	192 bp (0.038)	233 bp (0.363)	223 bp (0.408)	**230 bp (0.013)**	183 bp (0.184)
4	321 bp (0.386)	190 bp (0.432)	252 bp (0.338)	**167 bp (0.605)**	166 bp (0.059)	**216 bp (0.65)**	**194 bp (0.769)**	236 bp (0.113)	227 bp (0.08)	232 bp (0.025)	185 bp (0.237)
5	326 bp (0.143)	**194 bp (0.297)**	256 bp (0.243)	171 bp (0.25)	170 bp (0.015)		196 bp (0.064)	239 bp (0.012)	231 bp (0.039)	234 bp (0.05)	187 bp (0.211)
6	331 bp (0.014)	198 bp (0.041)	**260 bp (0.135)**	175 bp (0.026)			198 bp (0.052)		251 bp (0.025)	236 bp (0.063)	**189 bp (0.158)**
7	336 bp (0.014)		264 bp (0.027)							238 bp (0.087)	
8	341 bp (0.014)									**242 bp (0.288)**	
9										246 bp (0.175)	
10										250 bp (0.087)	
11										254 bp (0.113)	
12										260 bp (0.025)	
13										264 bp (0.013)	

Alleles shared among 16q-linked ADCA type III are highlighted in bold
PCR, Polymerase chain reaction; ADCA III, autosomal dominant cerebellar ataxia type III

physical map of the candidate interval, we now know that the entire length of the interval is no more than 4.8 Mb, and we further refined the critical interval of 16q-linked ADCA type III by the exact order of DNA markers shared among our affected individuals.

By applying the RepeatMasker program, we discovered 11 new highly polymorphic DNA markers that could be used to analyze haplotypes in our eight families. In the present study, we added two new 16q-linked ADCA type III families for haplotype analysis. This allowed us to further narrow a critical interval that shows a common, "founder" haplotype flanked by GGAA05 and D16S3095. The size of this new critical region was estimated to be 3.8 Mb. The present finding not only refines the candidate interval of this disease, but also corroborates our previous finding of a founder effect in the Japanese families with 16q-linked ADCA type III. In addition, analysis of this common haplotype would be useful for the molecular diagnosis of 16q-linked ADCA type III, which was previously diagnosed only with linkage analysis. Because large informative families are fairly uncommon for such a late-onset disease, finding a diagnostic haplotype would be important.

After refining the critical interval, we next searched a causative mutation in our patients. Because 16q-linked ADCA type III showed a mild phenomenon of anticipation, in that difference in the age-of-onset between parents and offsprings was 4.9 years (Nagaoka et al. 2002), we first searched for an expansion of trinucleotide CAG/CTG repeats detected by the software RepeatMasker, although none of the nine CAG/CTG repeats in the entire candidate region were expanded. When we tested the threshold of detecting CAG/CTG repeat sequence by the RepeatMasker program, we found that the program faithfully detected CAG/CTG repeats with more than six repeat units. Therefore, it seems probable that the CAG/CTG repeat, which has at least six repeat units in the normal population, is not expanded in our patients with 16q-linked ADCA type III. The smallest CAG/CTG repeats that are known to cause human neurodegenerative disease are the SCA6 gene and the myotonin protein kinase (*MtPK*) gene (Strachan and Read 1996; Zhuchenko et al. 1997; Ishikawa et al. 1997). These repeats are as small as 4 to 6 repeats in the normal population, and they expand to more than 20 repeats in SCA6 and more than 50 repeats in myotonic dystrophy type 1 (Strachan and Read 1996; Zhuchenko et al. 1997; Ishikawa et al. 1997). Considering that the threshold of detecting CAG/CTG repeats in our system is high, the present finding might indicate that the cause of the 16q-linked ADCA type III is not the expansion of the CAG/CTG repeat.

We also searched for any expansion of tri-, tetra-, penta-, or hexanucleotide repeats, as the ATTCT repeat expansion in SCA10 or the complex CCTG repeat expansion in myotonic dystrophy type 2 (Liquori et al. 2001). However, we did not observe any expansion of repeat sequences among a group of repeats that showed polymorphism in the general population. These observations further indicate that 16q-ADCA type III may be caused by a mutation other than a repeat expansion, such as a missense